# A NOVEL INDIRECT CONTROL METHODOLOGY FOR LOAD-LEVELING OF SPACE HEATING APPLIANCES

A thesis presented to the faculty of the Graduate School of Western Carolina University in partial fulfillment of the requirements for the degree of Master of Science in Technology.

By

Lee Thomas Holland

Director: Dr. Bora Karayaka
Assistant Professor
Department of Engineering and Technology

Committee Members: Dr. Aaron Ball, Department of Engineering and Technology
Dr. Martin Tanaka, Department of Engineering and Technology

July 2014

This thesis is dedicated to my parents.

# ACKNOWLEDGEMENTS

I would like to thank my major advisor, Dr. Bora Karayaka. Thank you for the guidance and encouragement throughout my graduate studies that has allowed me to have an appreciation and understanding of the subject matter required for writing this thesis.

Many thanks to my committee members Dr. Aaron Ball and Dr. Martin Tanaka for their expertise and encouragement. Great thanks to Dr. Yanjun Yan, Dr. Robert Adams, Dr. Paul Yanik and all other faculty members for their continued expertise and project help.

I would also like to thank Dr. James Z. Zhang and Dr. Patrick Gardner and the Center for Rapid Product Realization at Western Carolina University for the project support.

TABLE OF CONTENTS

LIST OF TABLES

LIST OF FIGURES

# ABSTRACT

A NOVEL INDIRECT CONTROL METHODOLOGY FOR LOAD-LEVELING OF SPACE HEATING APPLIANCES

Lee Thomas Holland, M.S.T.

Western Carolina University (July 2014)

Director: Dr. Bora Karayaka

Demand Side Management (DSM) programs provide utility companies with a method to shift consumer electricity usages away from peak electricity hours. DSM programs use alternative appliance usage schemes that maintain their usefulness while providing ancillary services for utilities. This thesis aims to develop a linear control methodology that can provide significant ancillary services for utilities without reducing customer comfort.

A prototype enclosure was built and equipped with a heater and thermal measuring equipment. Data was collected during a 17 hour temperature regulation experiment using a bang-bang controller similar to those commonly used for residential heating control. An experimental thermal system identification methodology was developed for online system identification. First and second order mathematical models were developed for thermal system identification. The mathematical models were calibrated using data collected experimentally and used to estimate the net thermal resistance and capacitance using system identification techniques.

The enclosure system model was also used to determine if peak power could be reduced by slowly varying loads utilizing a different type of controller. Two different linear control techniques (using K-Factor and PI approaches) and the associated power electronics circuitry were implemented and tuned in PSpice platform. Both

controller systems successfully leveled the load and reduced the peak power demand.

Finally the prototype enclosure was modified to include a linear controller using an available DC power supply and a buck converter power stage. The PI control scheme was used with a $60^\circ$ phase margin for smoother and faster settling characteristics. The phase margin was acquired using appropriate linear approximation of system transfer functions. The temperature response of the experimental system was compared to theoretical responses.

# CHAPTER 1: INTRODUCTION

## 1.1 Problem Statement

Utility companies adjust electricity generation to meet demand. During the summer afternoon typically, demand is at it's highest and this is called peak demand. In order to meet peak demand electricity generation is scheduled. Elaborate utility programs have been successfully implemented to reduce peak power levels. The reason for desiring to reduce peak demand is that the peak power is expensive to generate or purchase from other utilities.

Traditionally utilities meet peak demands by adjusting generation or purchasing electricity from other utility companies. For generation there are two main types of power plant. Base load plants typically provide $35 - 40\%$ of the maximum power for a given system. Base load generators attempt to be continuous, reliable, efficient, and have low costs. Coal is an example base load power plant with a ramp rate of $6 - 8$ hours. Solar and wind power plants are also considered base load because they cannot be controlled by utilities. Peak load power plants have very fast ramp rates and are typically operated $10 - 15\%$ of the time [1]. Hydro plants are the fastest peak load power plant, they can respond to control signals within a few seconds. Gas-fired peak plants respond between $10 - 30$ minutes [2].

The load factor of a power system is an important consideration for generation planning. Load factor is a ratio between peak energy usage, and average usage. Utilities desire a 1:1 load factor ratio. There are two primary method's utilities have implemented to improve load factor. First, pricing tariff's have encouraged consumers to shift electricity usage away from peak hours with opportunities to save electricity costs. Secondly, utilities have implemented direct control methods such as DSM or

DR to allow consumer appliances to be controlled by utilities with certain rules that attempt to balance customer comfort with cost savings.

## 1.2 Background on DSM and DR

By definition DSM refers to active efforts by utility companies to modify customers' energy use patterns. Demand Response (DR) programs are a type of DSM that respond to utility incentive programs or electricity pricing tariffs. Historically DSM was pioneered in the $1970s$ and $1980s$ due to concerns about dependence on foreign sources of oil. Environmental impacts of generating electricity were also heightened due to the nuclear reactor disaster at Three Mile Island in 1979. DSM programs were pioneered in the $1970s$ in order to change how much electricity is used and when electricity is used. DSM spending peaked in 1993 with 2.7 billion dollars being spent annually. With the large DSM spending utilities caused large energy savings with modest investments. For example, with 380 million dollars of utility spending $2360GWh$ of energy was saved in one year, corresponding to a price of almost 16 cents per $kWh$. The original price of generating energy without the DSM program would only be 3.2 cents for each $kWh$ of energy [3]. Since 1993 utilities have evaluated whether it is profitable to use DSM programs.

However, increased rollout of "smart meters" and added wind and solar generation have created a platform for DSM growth [4]. There are two primary methods to implement DSM that are described in this chapter. Electricity pricing tariffs can be implemented with smart meters to allow utilities to directly link end-users with the wholesale energy market. Control techniques allow end-users or utilities to modify electricity usage to reduce peak energy usage and improve system stability.

### 1.2.1 Electricity Pricing Tariffs

Utilities' fundamental operation problem is to keep the produced and con-

Table 1.1: Pricing Strategies in North America

| Structure | Time of Day of Day | Cost (Cents per kWh) | Additional Information |
|---|---|---|---|
| Flat Rate | | 6 | First $600kWh$ of Summer |
| (FR) | | 7 | Additional Use |
| Time of Use | $10pm - 7am$ | 4 | off-peak |
| (TOU) | $7am - 11am$ | 8 | mid-peak |
| | $11am - 5pm$ | 11 | on-peak |
| Critical Peak Pricing | $10pm - 7am$ | 3 | off-peak |
| (CPP) | $7am - 11am$ $5pm - 10pm$ | 8 | mid-peak |
| | $11am - 5pm$ | 11 | on-peak |

sumed power balanced at all times. Utilities must plan electricity generation based on day-ahead markets, where electricity is purchased in wholesale markets from generators and ultimately sold to end-use customers. End-use customers are shielded from short-term market decisions with traditional electricity pricing. Wholesale electricity prices experience spikes when equipment failures occur typically in generators or transmission lines. Different pricing techniques have been implemented to expose end-use customers to the risks of managing wholesale energy prices [4].

In Table 1.1 a review of recently implemented electricity pricing strategies in North America has been performed. For these pricing strategies smart meters are needed to record electricity usage on at least an hourly basis. Notably time-of-use (TOU) and critical peak pricing (CPP) provide predefined electricity prices for periods of times. These programs are identical with the exception that CPP has event days that are advertised a day in advance. On event days electricity prices are very large for $3-4$ hours. For real time pricing (RTP) electricity prices change every hour depending on the price of electricity for a given wholesale market [5].

### 1.2.2 Control for DSM and DR Techniques

Direct Load Control (DLC) DSM strategies are generally performed with thermostatically controlled appliances (TCA's) in order to be able to stop using a load when needed. Thermal momentum in TCA's allows control to be temporarily delayed. DLC programs do not attempt to reduce energy usage. For DLC programs it is common to have hardware that senses power output of a given appliance, on/off cycles, input/output interfacing with loads, and hardware that directly controls the load. Software at a central utility location identifies the load model in order to generate control actions [6]. Another control method used in DSM is called indirect load control (ILC). In this method, the power consumption of loads is controlled manually by the customers or automatically by the appliances. ILC programs can respond to electricity pricing schemes by adjusting to day ahead pricing or other electricity pricing tariffs [7].

Thermostatically controlled appliances (TCA's) that are targeted for control include space heaters, electric water heaters (EWH's), and other appliances with a power ratings less than $10kW$ [8]. TCA's can respond quickly to control, and can have thermal time constants above 15 minutes. TCA's have a thermal momentum that is traditionally maintained at a desired temperature set-point. There are three primary techniques to use TCA's for DSM. First, changing the temperature set-point during peak hours. Second, prioritizing TCA power need can allow for queuing that can shift power usage from peak hours without reducing customer comfort. Third, modification to TCA controllers to reduce power demand which can achieve load shifting or reduction.

Changing the temperature set-point of consumer appliances has been implemented for air conditioner TCA's [9]. In the survey, customers that opt-in to the program are given free communicating thermostats. The program uses a direct load control (DLC) methodology, and installs equipment on the air conditioning units.

The DLC program can operate only on a predefined number of "event" days and is only used for a few hours on each day. The air conditioner for each house is used heavily after the event period is over, this is called "snap-back".

Queuing DLC programs can target individual appliances for control by utilities. Large aggregate pools of appliances are able to be actively controlled by utilities to improve load factor. In Lu et. al. [10], 1000 space heaters are simulated with a queuing DLC strategy. Heaters are prioritized based on room temperature with the coldest rooms being energized first. One of the significant outcomes of this study is the ability for load regulation. Load regulation for this system would reduce variability in the aggregate power consumed. A simulation in Kondoh et. al. [7] used EWH's for load following with $33,000$ heaters. The EWH's are partially controlled centrally with switches that interrupted normal water heating when needed. To retain customer comfort, EWH's were allowed to heat water when the top thermostat is active. The EWH control circuit is modified to allow a thermostat to be controlled by the utility, two-way communication is also utilized.

Finally adding non-centralized controllers to TCA's has been proposed for DSM. In Nehrir et. al. [11], simulations are performed for 1000 EWH's with different power levels that are changed from $110V/120V$ to $220V/240V$ based on utility control. Changing power could also be performed with heating elements of different sizes. One simulation showed that large power oscillations can occur when the appliances have similar insulation and volume. Another simulation showed that minimizing the EWH heating element power can reduce peak power usage without reducing customer comfort.

A DR program has been proposed by Baghina et. al. [12]. The DR program uses a model predictive controller to create a day-ahead energy usage schedule. A day-ahead energy market is also utilized to attempt to save the customer money. The

paper found that freezers can provide short-term DR, but can accidentally become synchronized causing aggregate power consumption to be higher at certain moments.

Nikolai et. al. [13], performed a study where EWH's and air conditioners are targeted for DR by adding small open-loop controllers to appliances that respond to a one-way communication signal from utilities. The study simulated large aggregates of TCA's being turned on or off for a period of time. When the TCA's are turned back on large oscillations of power occur. The paper proposes several protocols to reduce oscillations and provide regulation services for utilities to increase system stability.

### 1.2.3 Space Heating's Potential for DSM and DR

One large target for load factor improvement is space heating appliances and other Thermostatically Controlled Appliances (TCAs). In 2009, space heating accounted for over 40% of all residential energy usage [14]. Electric space heating consumption by 2030 is projected to be $164TWh$ and potential consumption savings through various technology implementations can be as high as $28TWh$ [15]. Also, the US, single family residential houses consume up to 66% of their energy from controllable appliances [16]. Controllable appliances also include electric water heaters, ovens, air conditioners, refrigerators, and dishwashers.

## 1.3 Bang-Bang Control Background

Bang-bang control definitely has a negative impact on load factor and ramp rates due to the large variations in demand. In bang-bang or on/off control the electric heater is turned on to maximum power until a set-point is reached with an acceptable overshoot. Once the set-point is achieved, the heater turns completely off until the room temperature cools below an error threshold and then turns the heater back on.

Space heaters are typically operated with bang-bang control. There is a trade

off between switching times and steady-state accuracy for space heaters. Increasing the switching frequency reduces the overshoot/undershoot of a thermostat but causes undesirable transients for utilities [10]. One undesirable feature of common nichrome electric heating elements is inrush current that occurs on each heating cycle. Inrush currents occur due to $0 - 10\%$ smaller resistances at room temperature as opposed to when hot. [17]

## 1.4 Proposed Strategy

In this thesis an experimental space heater control methodology is proposed that could be used to provide DSM services. The space heater controller proposed is an ILC scheme where control actions are made automatically by the appliance. This controller simply replaces end-user thermostatic bang-bang controllers. The power is controlled through electronic means to match a room's heating requirements to the thermal power provided. Previous research has shown that loads smaller than $10kW$ can effectively provide ancillary services [8]. The objectives of this thesis include:

- Reduce peak demand
- Smoother demand ramp rates

This thesis proposes a novel DSM scheme that can significantly reduce the peak power used for space heating, and provide ancillary services to the utility. An identification study using a Least Squares estimation technique was first performed on an experimentally heated space. Simulations were later performed utilizing PI and K-Factor control approaches on this identified thermal model [18]. Finally the physical thermal system is controlled with a linear buck converter power stage and temperature responses were compared to theoretical simulations.

In this thesis, a novel experimental methodology is presented that relates the thermal model to the electrical power supplied. The ultimate goal is to develop an intelligent controller that automatically detects the system thermal parameters using the system identification methods proposed here and uses these parameters for adaptive load regulation.

The thesis is organized as follows: Chapter 2 is the motivation for this research. Chapter 3 introduces two stages of methodology needed for the project. The results of the experiment are shown in Chapter 4. An overall summary is performed in Chapter 5 with a glance at future works.

# CHAPTER 2: MOTIVATION

In order to rationalize the development of a linear controller for a space heater peak power reduction is targeted with the implementation of a smooth linear power signal. A statistical analysis is performed using a binomial distribution to model bang-bang space heaters. A simulation is performed for aggregate bang-bang and linear space heaters using similar power levels. Peak power is compared for each aggregate. A 1% probability is analyzed using the binomial distribution to calculate the peak power reduction difference between the two aggregates with total and per unit calculations.

A linear control scheme can reduce the peak power of individual loads and reduce power ramp rates at the same time. Aggregated leveled loads always maintain a more consistent load when compared to bang-bang systems. For example, the probability distribution function (PDF) for aggregated demand of 100 space heater loads operated in bang-bang fashion can be seen in Fig. 2.1. In this specific example, the space heaters all are assumed to have the same duty cycle of 50%.

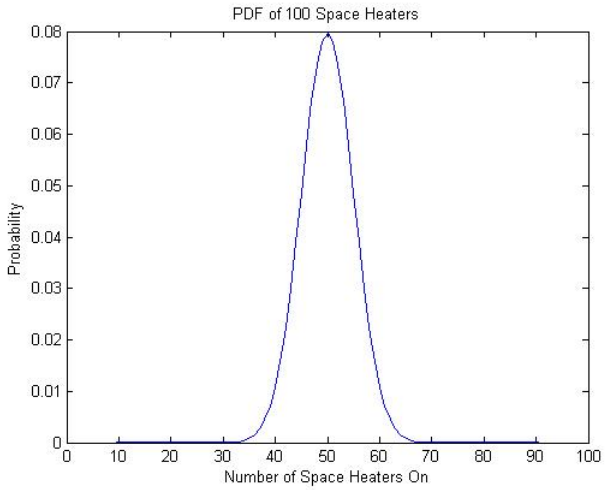


Figure 2.1: PDF for 100 aggregated space heaters with 50% duty cycle

In addition, the starting times for each heater are uniformly distributed. From the PDF of Fig. 2.1 one can easily deduct that the greatest probability is having 50 space heaters on at any given time. However, it is also probable that more than 60 heaters can be on at any given time. A simulation was performed for 100 space heaters with a power rating of $10kW$ for each when turned on. The voltage rating was $120V$ for each heater, while the current rating from power and voltage calculations was found to be $83.33A$. All of the space heaters were given a 50% duty cycle, and simulations were performed using two 1000 second cycles of each heater. In order to add variation to the experiment the starting times were randomized using a uniform distribution, the start time could occur at any time during the $1000s$ period. When a space heater turns on after $500s$ in each period the 50% duty cycle is maintained by mirroring the remaining power to the beginning of the period. An example plot with a mirrored heating cycle can be seen in Fig. 2.2.

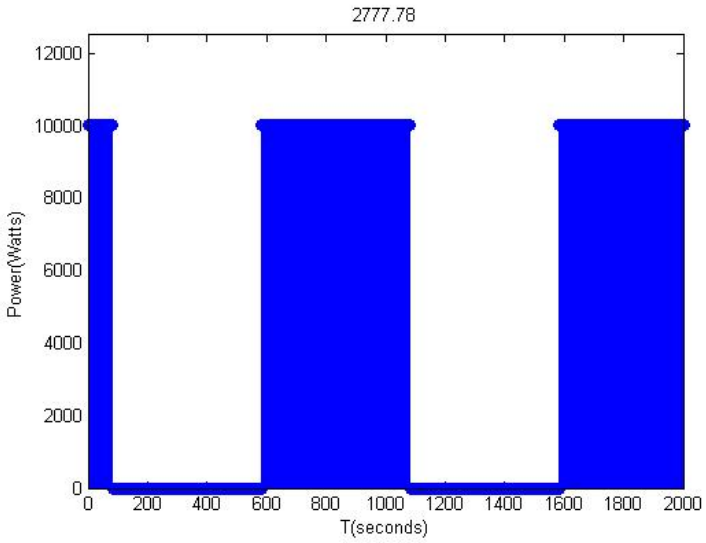


Figure 2.2: Single Bang-Bang heater with mirrored duty cycle

A leveled control simulation was also performed and compared to the bang-bang simulation. A constant voltage and current was used for convenience resulting in all space heaters having consistent heating plots. To compare the two simulations,

each group was summed into one data set showing the entire power load for a utility company. The bang-bang aggregate plot gives a peak power value of $580kW$ while the load leveling controller gives a consistent $500kW$. The bang-bang and linear aggregate plot can be seen in Fig. 2.3.

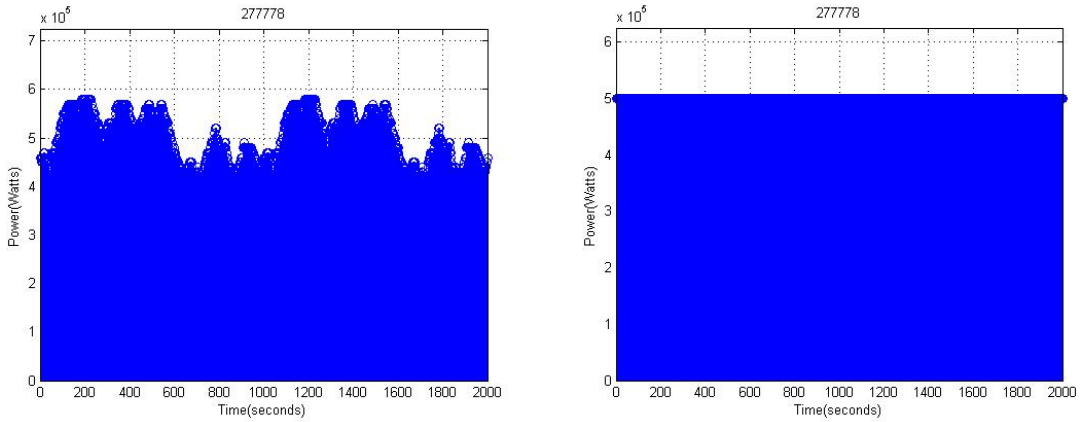


(a) Bang-Bang (b) Linear

Figure 2.3: Aggregate Power of 100 Space Heaters

A histogram with 100 bins can also be seen in Fig. 2.4 for the bang-bang and load leveling controllers. The bang-bang histogram has a varied power levels from 420 to $580kW$ with a peak number of samples at $430kW$ and $570kW$. On the other hand, the leveled control histogram has a fixed power level of $500kW$ for all the samples

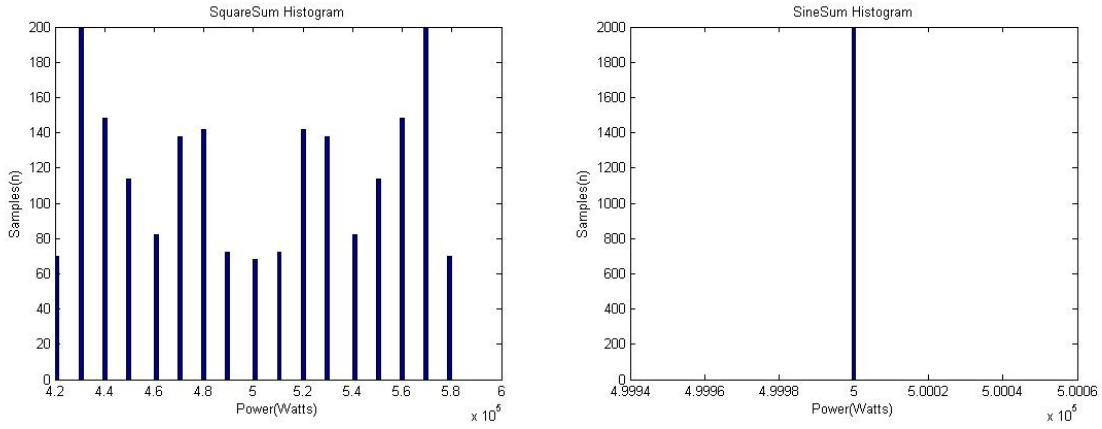


(a) Bang-Bang (b) Linear

Figure 2.4: Histogram of 100 Aggregated Heaters

which correspond to a reduction of more than 13% in comparison to $580kW$.

A sample aggregation was also performed using $10kW$ space heaters with a constant 50% duty cycle. Peak power reduction can be seen in Table 2.1. A 1% probability criteria of occurrence for each cycle was used with a binomial cumulative distribution function. The peak power reduction increases with the number of appliances used, but the per unit peak power savings reduces.

Table 2.1: Peak Power Reduction using Binomial CDF

| Number of Units | Peak Power Reduction kW | Peak Power Reduction Per Appliance kW |
|---|---|---|
| 100 | 124.9 | 1.24 |
| 1000 | 370 | 0.37 |
| 33000 | 2108 | 0.064 |

# CHAPTER 3: METHODOLOGY

## 3.1 Estimation

### 3.1.1 Thermal Circuit Equivalency

In order to determine individual space heater loads, a simple thermal characteristic model is needed to capture each buildings unique thermal heating characteristics. Thermal parameter estimation methods in the published literature utilize various estimation methods for space heating applications [19–21]. Thermal resistance networks are often used to estimate the rate of heat transfer through a system [22]. In these systems, the heat transfer, temperature, and thermal resistance are analogous to the current, voltage and electrical resistance of an equivalent electrical circuit, respectively. Energy storage in the air and other materials may be represented using capacitors, where $\frac{dU}{dt}$ is the change in internal thermal energy (kJ/s), $P_{in}$ is the power delivered to the room by the electric heating element (W), and $\dot{Q}_{out}$ is the heat loss through the walls of the building (W).

Energy balance in a thermal system can be described by (3.1)

$$\frac{dU}{dt} = P_{in} - \dot{Q}_{out} \tag{3.1}$$

An increase in internal thermal energy results in an increase in temperature according to (3.2). The mass of the thermal system is represented by $m$ $(kg)$, $c_p$ is the specific heat capacity $(\frac{kJ}{kgK})$, and T is the system temperature (K).

$$\frac{dT}{dt} = \frac{1}{mc_p}\frac{dU}{dt} \tag{3.2}$$

Total heat transfer is estimated by (3.3). $R_{tot}$ is the total thermal resistance. $R_{tot}$ can account for any combination of convective and conductive heat transfer components. Combining equations (3.1), (3.2), and (3.3) yields (3.4).

$$\dot{Q}_{out} = \frac{T_{room} - T_{outside}}{R_{tot}} \tag{3.3}$$

$$P_{in} = \frac{T_{room} - T_{outside}}{R_{tot}} + mc_p \frac{dT_{room}}{dt} \tag{3.4}$$

Two models were developed to represent the thermal dynamics using an electrical circuit analogy. The first is a first order circuit model with a single thermal capacitance (Fig. 3.1). The circuit dynamics in state space form can be seen in (3.5). In the system $x$ is the state variable representing room temperature $T_{room}$ and $y$ is the system output of $T_{room}$ that is measurable. $V_1$ is the input representing ambient temperature $T_{ambient}$ or $T_{outside}$. $P_{in}$ is the second input for electrical power supplied. $R_1$ and $R_2$ are the thermal resistances for heaters and enclosure, respectively. $C_1$ models the combined thermal mass or capacitance which is the same as $mc_p$ in equation (3.4).

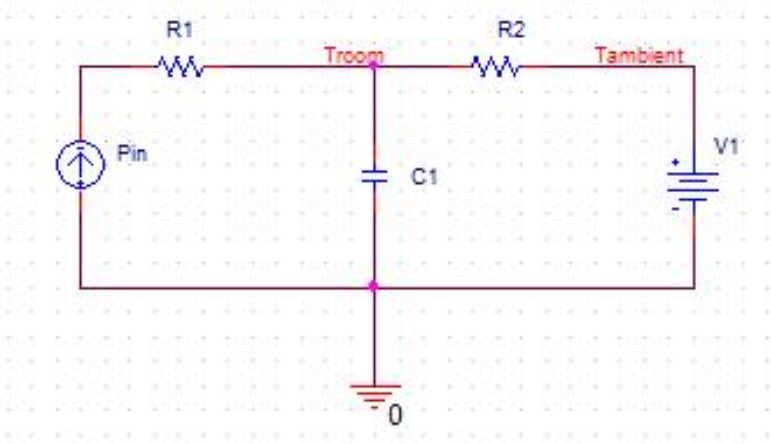


Figure 3.1: First Order Thermal Circuit Model

$$\dot{x} = -\frac{x}{R_2C_1} + \frac{V_1}{R_2C_1} + \frac{P_{in}}{C_1} \tag{3.5}$$
$$y = x$$

The second is a model with two thermal capacitance levels that also incorporates heater dynamics (Fig. 3.2). The circuit model in state space form is shown in (3.6). Where $x_1$ and $x_2$ are the state variables that represent heater temperature $T_{heater}$ and room temperature $T_{room}$, respectively. The variable $y$ is the system output $T_{room}$ that is measurable. $V_1$ is the input that represents ambient temperature $T_{ambient}$. $P_{in}$ is the second input for electrical power supplied. $R_1$, $R_2$ and $R_3$ are the thermal resistances for heater, air and enclosure. The capacitor ($C_1$) and ($C_2$) are used to model combined heater and air thermal capacitances in the room.

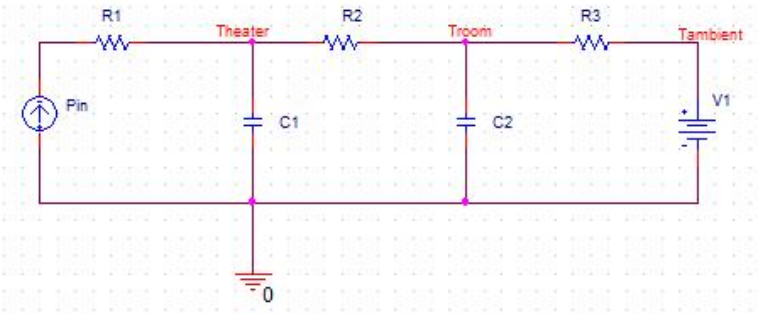


Figure 3.2: Second Order Thermal Circuit Model

$$\begin{pmatrix} \dot{x}_1 \\ \dot{x}_2 \end{pmatrix} = \begin{pmatrix} \frac{-1}{R_2C_1} & \frac{1}{R_2C_1} \\ \frac{1}{R_2C_2} & \frac{-1}{R_2C_2} - \frac{1}{R_3C_2} \end{pmatrix} \begin{pmatrix} x_1 \\ x_2 \end{pmatrix} \begin{pmatrix} 0 \\ \frac{1}{R_3C_2} \end{pmatrix} V_1 + \begin{pmatrix} \frac{1}{C_1} \\ 0 \end{pmatrix} P_{in} \tag{3.6}$$
$$y = x_2$$

### 3.1.2 Estimation Methodology

The estimation method utilizes a cost function V to minimize error. This cost function can be stated in (3.7).

$$V(\hat{\theta}) = \frac{1}{N}\Sigma_{k=0}^{N}\left[e^T(k,\hat{\theta})e(k,\hat{\theta})\right] \tag{3.7}$$

In the equation $\hat{\theta}$ is the parameter vector to be estimated, $N$ is the number of samples, and $e$ is the error between estimated and measured output values. $e$ is defined with (3.8) where $Y(k)$ and $\hat{Y}(k)$ are the system and the model outputs, respectively (Fig. 3.3). The cost function $V$ can be effectively minimized by using an adaptive version of Gauss-Newton (GNA) [23] and Levenberg-Marquardt (LM) [24] least squares search algorithms.

$$e(k) = Y(k) - \hat{Y}(k) \tag{3.8}$$

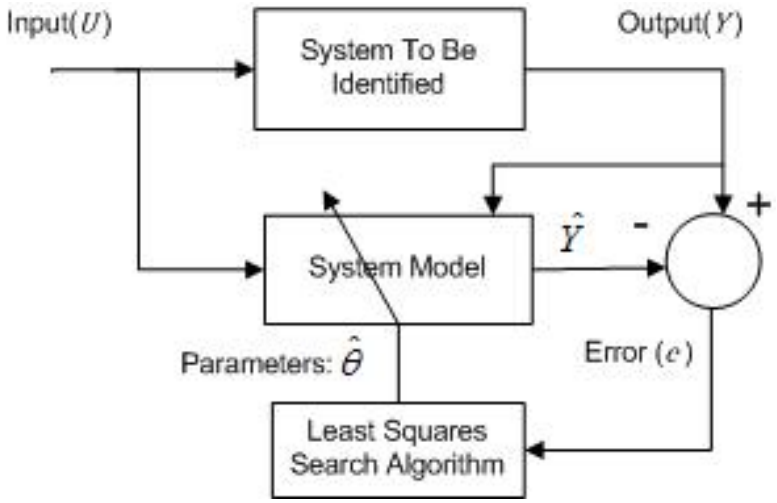


Figure 3.3: Parameter Estimation Scheme

The parameter estimation vector is $\hat{\theta} = [R_2\ C_1]$ for the first order model (3.5) and $\hat{\theta} = [R_2\ C_1\ R_3\ C_2]$ for the second order model (3.6) . The input vector is $U = [P_{in}\ T_{ambient}]$ and the output vector $Y = T_{room}$. Since $R_1$ is not part of models (3.5) and (3.6), it cannot be estimated.

### 3.1.3 Test Setup and Data Collection

In order to perform system identification, the temperature and power were measured over time to obtain the input-output relationship (Fig. 3.3). A prototype insulated enclosure with a built in heater was constructed (Fig. 3.4). The enclosure did not have insulation on the bottom. Using the input power data and the thermal boundary temperatures, system identification was used to determine the thermal capacitance of each system model and the total thermal resistance of each thermal boundary surface.

Figure 3.4: Thermal Enclosure Used for Estimation

### 3.1.4 Data Collection

Input power and temperature was monitored using a custom $LabVIEW^{TM}$ program as outlined in Fig. 3.5. A full $LabVIEW^{TM}$ block diagram is shown in Fig. A.1 of the Appendix. Power levels were read via the Visa Serial Communication port. A serial command was written for external data logging with a 1 second time interval. Data was then read with a Visa read node whenever a serial command was sent from the power meter. The NI 9219 Module was used with a $cDAQ-9172$ to read four Honeywell $td5a^{TM}$ three-wire RTD temperature sensors. One sensor was used to measure the room ambient temperature, and three sensors located inside the

enclosure at the door, floor, and heater were used to monitor the temperatures of these components (Fig. 3.4). The RTDs utilized a $5V$ external source and a voltage divider application circuit that yielded an accuracy of $\pm 0.4\,^{\circ}\mathrm{C}$. The voltage across the RTD changed with the temperature and was converted to temperature in Celsius after the data was collected. Power and temperature data was saved to an ASCII text file.

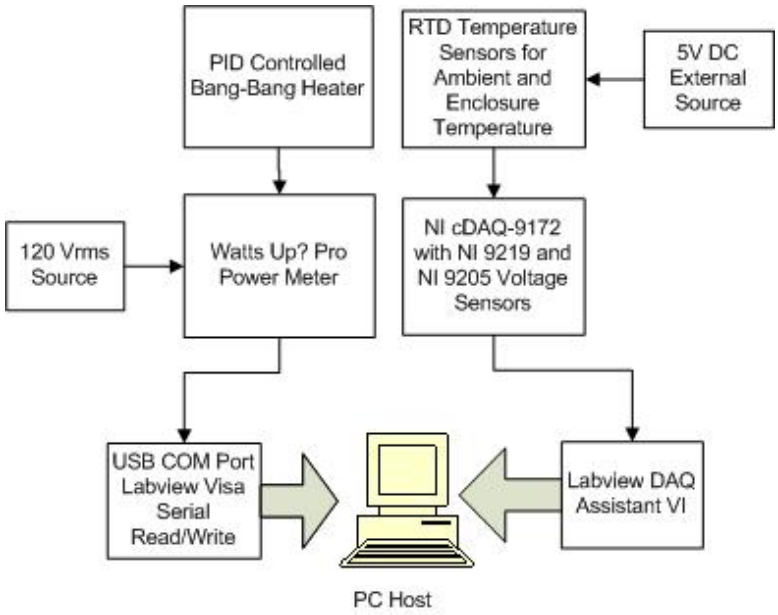


Figure 3.5: Data Acquisition Block Diagram

### 3.1.5 Testing Procedure

The testing procedure used a Love Controls Series 16A PID controller that utilized a standard bang-bang controller (turn on/off). The on temperature was set at $28.6\,^{\circ}\mathrm{C}$ and the off temperature was set at $32.1\,^{\circ}\mathrm{C}$. The controller used a thermocouple sensor located in the close proximity to the RTD door sensor (Fig. 3.4). This test was performed without a bottom insulation and generally uniform insulation on the inner walls. During this test, the data was continuously collected for over 17 hours. The electric power readings were sampled each second and temperature readings were sampled every 1.8 seconds. In order to be consistent for the estimation procedure,

the data acquired was reorganized and up-sampled at 2 sec intervals for both temperature and power readings.

### 3.1.6 Results

The measured data for temperature and electric power readings can be seen in Fig. 3.6. The first 10,000 seconds of data were removed from the analysis in order to allow the temperature to reach steady state. A total of seven thousand data points (14,000 s) were used in the estimation procedure and the rest of the data were reserved for validation. Throughout the estimation process a function that measures the quality of fit between estimated and measured data was utilized [25] (3.9) where $Y$ is measured data and $\hat{Y}$ is estimated model output, and the mean function denotes the mean value of the array. The first order thermal model given by (3.6) was used to estimate $R_2$ and $C_1$. Without a-priori knowledge about the physical parameters, the initial values for $R_2$ and $C_1$ were randomly selected as $0.15\frac{^\circ\text{C}}{W}$ and $15,000\frac{W-sec}{^\circ\text{C}}$, respectively, to begin the search.

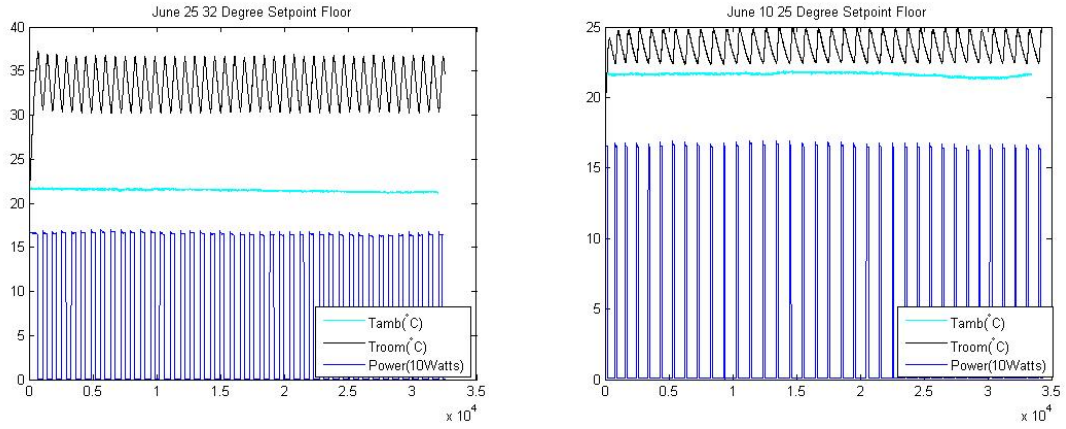


(a) 32 °C (b) 25 °C

Figure 3.6: Temperature and Power Data Collected for Both Set-points Using Door Sensor

Table 3.1: First Order Thermal Estimation and Validation Results

| Set-point °C | $C_1$ $\frac{W-sec}{°C}$ | $R_2$ $\frac{°C}{W}$ | Estimation % | Validation % |
|---|---|---|---|---|
| 25 | 20411 | 0.0798 | 40.64 | 39.24 |
| 32 | 92970 | 0.078 | 48.39 | −33.90 |

$$fit(\%) = 100\left(1 - \frac{\sqrt{\Sigma_{k=1}^{n}(Y(k) - \hat{Y}(k))^2}}{\sqrt{\Sigma_{k=1}^{n}(Y(k) - mean(Y))^2}}\right) \tag{3.9}$$

The system was identified with both first and second order thermal models. Both 25 °C and 32 °C set-points were originally estimated for each circuit model. Estimations were performed with samples 5000 through 12000 and validated using samples 12000 through 32000. First order estimation and validations for 25 °C and 32 °C can be seen in Fig. 3.7, 3.8, 3.9 , and 3.10. A table showing the first order estimation results can be found in Table 3.1. All estimations and validations in this thesis utilized data from the temperature sensor on the left door of the enclosure. An identification Matlab file can be found in Appendix A, with functions for both thermal models used in this thesis.

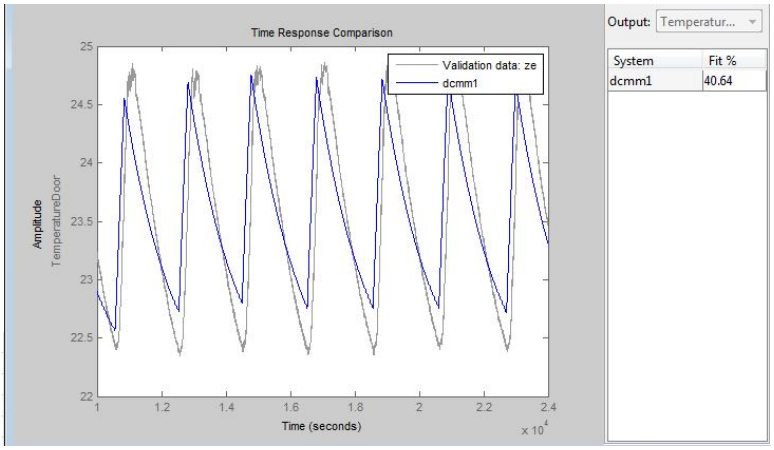


Figure 3.7: Thermal Estimation 25 Degree Set-point with First Order Thermal Model

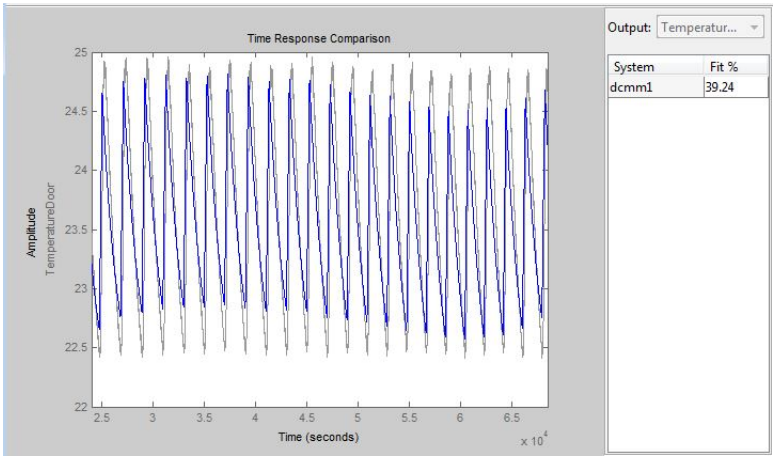


Figure 3.8: Thermal Validation 25 Degree Set-point with First Order Thermal Model

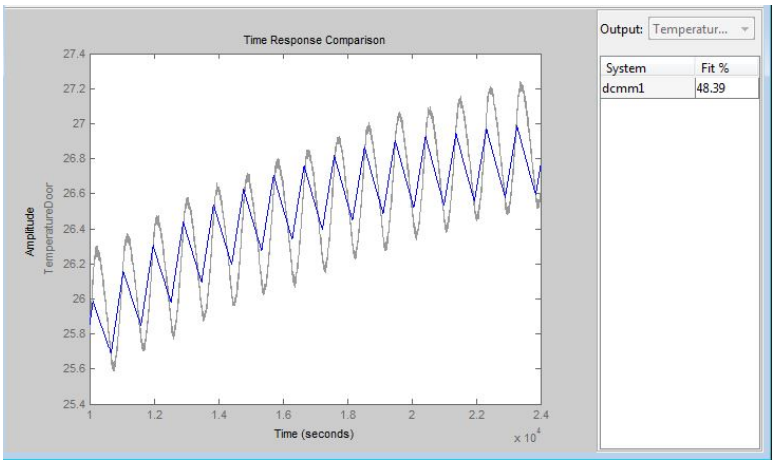


Figure 3.9: Thermal Estimation 32 Degree Set-point with First Order Thermal Model

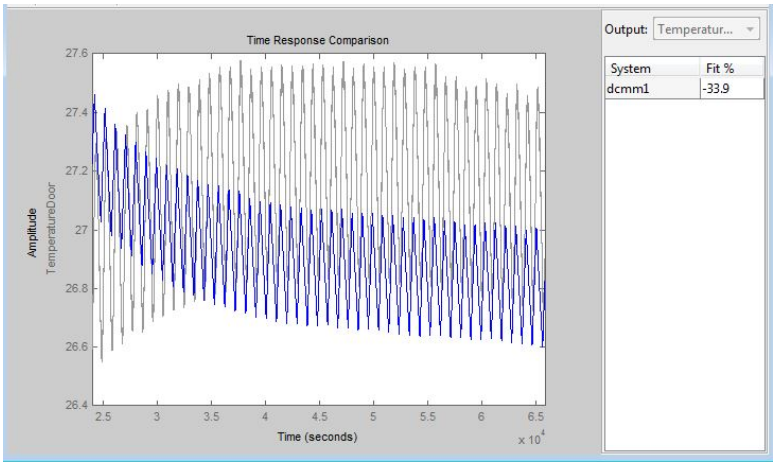


Figure 3.10: Thermal Validation 32 Degree Set-point with First Order Thermal Model

A second order estimation for 25 °C and 32 °C set-points was also performed using the same sample parameters. Second order estimation and validations for 25 °C and 32 °C can be seen in Fig. 3.11, 3.12, 3.13 , and 3.14. A table showing the first order estimation results can be found in Table 3.2.

The validation results also showed good agreement with estimated parameters of the second order model (Fig. 3.12, and 3.14). The final thermal parameters can be seen in Table 3.2. The estimated parameters from the 25 °C test are used in the experimental validation stage.

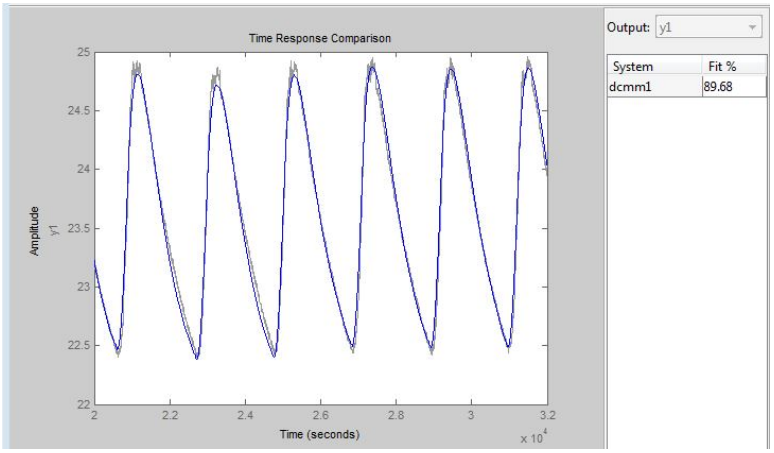


Figure 3.11: Thermal Estimation 25 Degree Set-point with Second Order Thermal Model

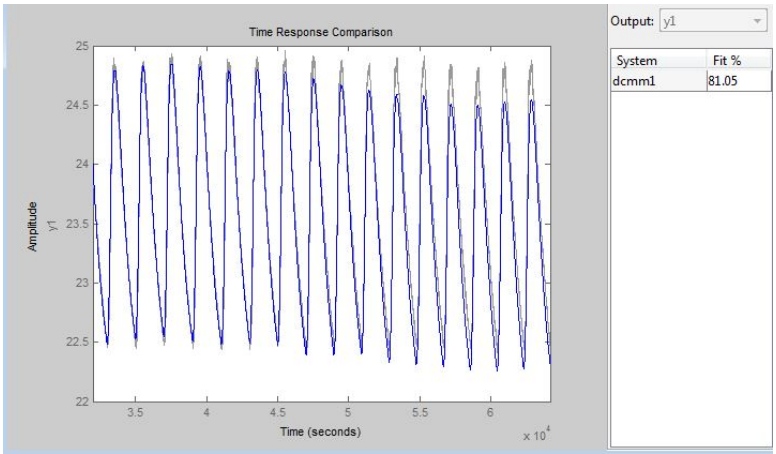


Figure 3.12: Thermal Validation 25 Degree Set-point with Second Order Thermal Model

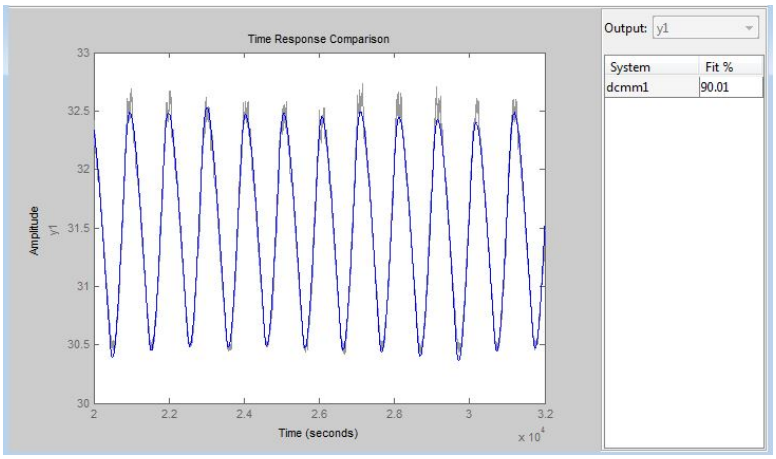


Figure 3.13: Thermal Estimation 32 Degree Set-point with Second Order Thermal Model

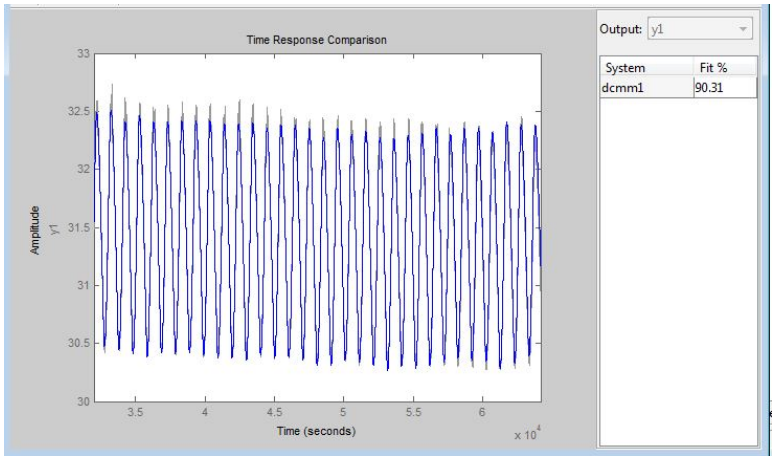


Figure 3.14: Thermal Validation 32 Degree Set-point with Second Order Thermal Model

Table 3.2: Second Order Thermal Estimation and Validation Results

| Set-point °C | $C_1$ $\frac{W-sec}{°C}$ | $C_2$ $\frac{W-sec}{°C}$ | $R_2$ $\frac{°C}{W}$ | $R_3$ $\frac{°C}{W}$ | Estimation % | Validation % |
|---|---|---|---|---|---|---|
| 25 | 120.67 | 3134.96 | 6.55 | 0.079 | 89.68 | 81.05 |
| 32 | 256.99 | 1297.92 | 5.98 | 0.14 | 90.01 | 90.31 |

## 3.2 Simulation

### 3.2.1 Lumped Capacitance Circuit Model

The thermal estimation was used to simulate both PI and lead compensator controllers. The thermal system from (3.6) was implemented into PSpice as seen in Fig. 3.15. Two second order thermal circuit equivalent systems were developed as seen in Table 3.2.

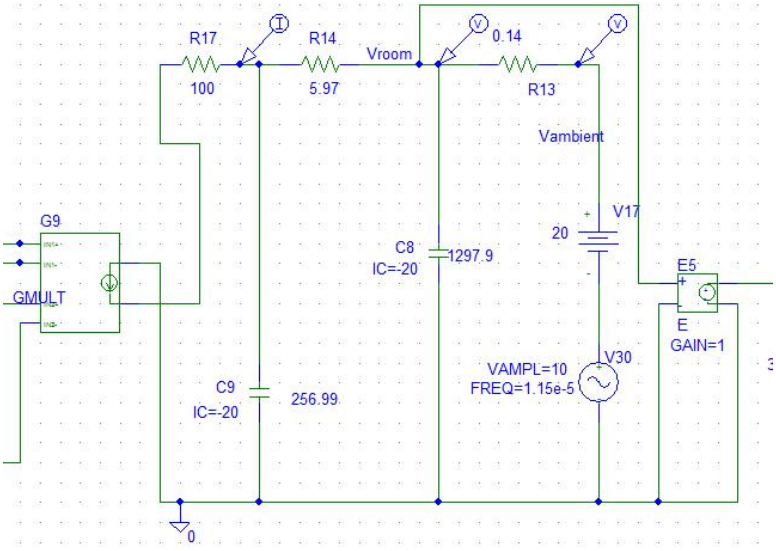


Figure 3.15: Two Capacitance Thermal Model Stage in PSpice

### 3.2.2 Control Methodology

A general control scheme was designed in the implementation of each controller. Steady state error is the set-point temperature, $T_{sp}$, minus the room temperature, $T_{room}$. The steady state error was used as feedback in the closed loop system (Fig. 3.16). In order to design the controller, a transfer function is needed for each

of the other system blocks. From the system identification study a thermal transfer function was found for both the 25 °C and 32 °C set-points. An example thermal system transfer function (with power input and room temperature output) can be seen in equation (3.10), where the state space model of the 32 °C system identification was converted to a transfer function using appropriate Matlab functions. The controller transfer function is different for each design and will be introduced accordingly.

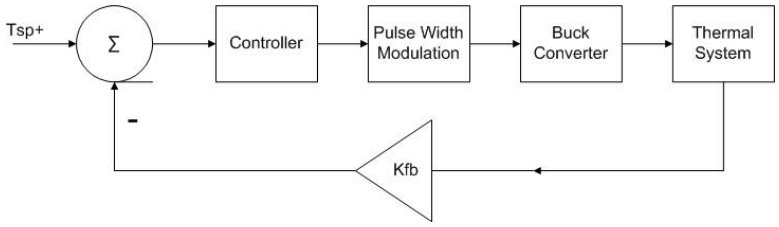


Figure 3.16: Controller Block Diagram

$$G_T(s) = \frac{5 \cdot 10^{-7}}{s^2 + 0.006s + 3.6 \cdot 10^{-6}} \tag{3.10}$$

Assuming the availability of AC-DC rectifier front end or direct DC power, a DC-DC buck converter power stage due to its near linear characteristics was adopted in the simulations. In order to match the power stage to the real system, a $120V$ DC input (120 $V_{rms}$ AC equivalent) was assumed, with an 87.53Ω heater load resistance. The linearized transfer function for the buck converter $G_{PS}(s)$ in this system can be seen in equation (3.11) [26].

$$G_{PS}(s) = \frac{V_{in}}{LC} \frac{1 + srC}{s^2 + s(\frac{1}{RC} + \frac{r}{L}) + \frac{1}{LC}} \tag{3.11}$$

In (3.11) $V_{in}$ is the input DC voltage, $L$ and $C$ are output filter inductor and capacitor and $r$ is the series leakage resistance for the filter capacitor. The input control signal to the buck converter is the duty cycle for the Pulse Width Modulation (PWM) which varies from 0 to 1, and the output is the voltage across the heating element resistance. The PWM block allows the controller to operate either in

Continuous Conduction Mode (CCM) or Discontinuous Conduction mode (DCM). To be able to provide continuous current and therefore to reduce the stress on the heating element, CCM would be the choice of operation. In practice, an IC-PWM chip needs to be chosen, and associated gain $K_{fb}$ needs to be determined. In our design, a unity $K_{fb}$ was chosen for the PI controller and bang-bang controller, and a $K_{fb} = 10$ was used for the Phase Boost controller.

### 3.2.3 Bang-Bang Control Strategies

In PSpice, this was simulated using a Schmitt Trigger circuit as seen in Fig. 3.17. The $R_{22}$ and $R_{23}$ values were chosen to give a +/ threshold of 1 °C. The set-point is centered between the upper and lower threshold, and can be adjusted by changing $V_{34}$ if desired.

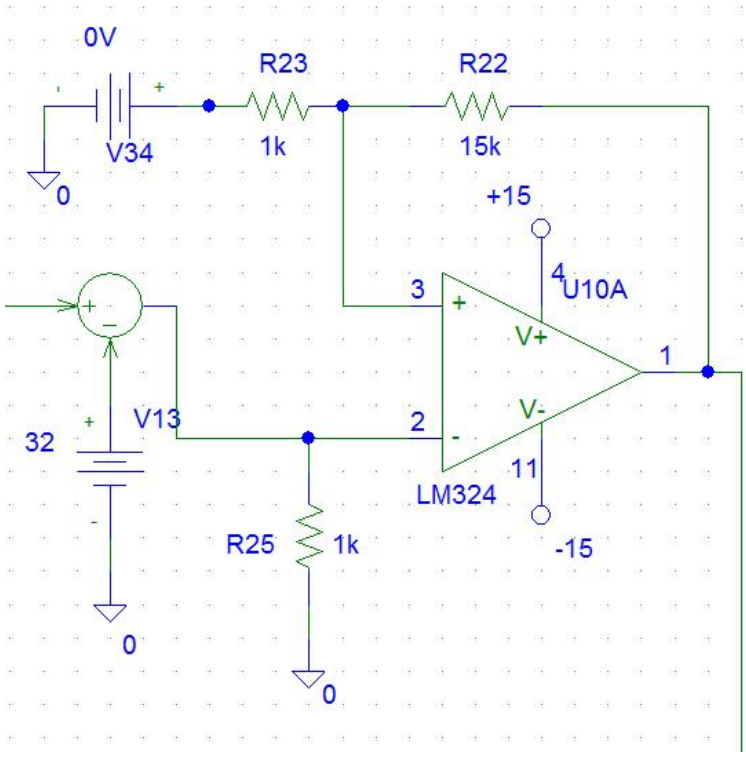


Figure 3.17: Bang-Bang Controller with Schmitt Trigger Stage

### 3.2.4 Linear Control Strategies for Space Heaters

The PWM stage used in the simulation of linear control strategies determines when the buck converter is in the active or cutoff operation mode. For this project, an ideal transformer was used to represent a MOSFET, and a limit function was used for the PWM stage. Also, $K_{fb}$ in Fig. 3.18 is the gain for the feedback loop before the limit function and should be chosen to give a maximum duty cycle of 100%. A review of voltage control systems can be found in [26].

### 3.2.5 Phase Boost Controllers (Lead Compensators)

The transfer function chosen for the controller can be seen in equation (3.12). The objectives when designing the controller were to maximize cross-over frequency $f_c$ for fast response, a $60\,^\circ$ phase margin for smooth settling, and a phase angle above $-180\,^\circ$ for all frequencies below crossover frequency. Matlab was used in conjunction with the transfer function of the complete system to choose a cutoff frequency that gives $60\,^\circ$ phase margin. The cutoff frequency is the point where the magnitude and phase of each transfer function are determined. Since it is desirable to have a zero or minimal steady state error, the controller should have a pole at the origin which means the introduction of a $-90\,^\circ$ phase angle in the open loop transfer function. The open loop transfer function phase for the system at $f_c$ is $\angle G_{OL}(s) = -120\,^\circ$ for $60\,^\circ$ phase margin. A phase boost is calculated using (3.12) to achieve this phase margin. The controller parameter values $k_c$, $\omega_z$ and $\omega_p$ can then be calculated based on the design steps in reference [26] .

$$G_C(s) = \frac{k_c}{s}\frac{(1+\frac{s}{w_z})}{(1+\frac{s}{w_p})} \tag{3.12}$$

$$\phi_{boost} = \angle G_{OL}(s) - \angle G_T(s) - \angle G_{PS}(s) + 90\,^\circ\mathrm{C} \tag{3.13}$$

A circuit schematic of the phase boost controller implementation along with thermal system and power stage can be seen in Fig. 3.18.

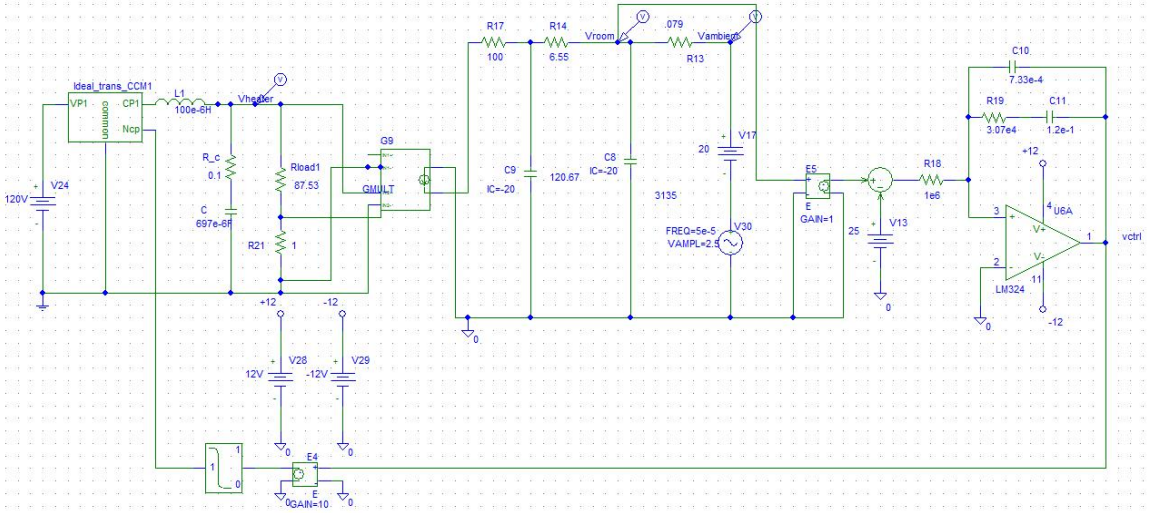


Figure 3.18: Phase Boost Controller PSpice Circuit

### 3.2.6 Proportional Integral Controller

A Proportional Integral (PI) controller was also tested with the thermal system. PI controllers allow steady-state error to approach zero, and fast convergence can be achieved when controller parameters are properly chosen. Also, PI controllers can be utilized for nonlinear system control applications. For this simulation a P-term: $Kp = 1$ and I-term: $Ki = 5e - 4$ were found for a satisfactory performance. The feedback gain $K_{fb}$ term was set to 1 for the PI controller. A PSpice circuit implementation for a PID controller can be seen in Fig. 3.19. The P-term is found from the ratio of $\frac{R_{31}}{R_{29}}$, while the I-term is found from the ratio of $\frac{C_{16}}{R_{29}}$ . The D-term of a PID controller is found using $C_{17}$ but is voided in this simulation with an open switch. The transfer function for the PID controller can be seen in Equation (3.14).

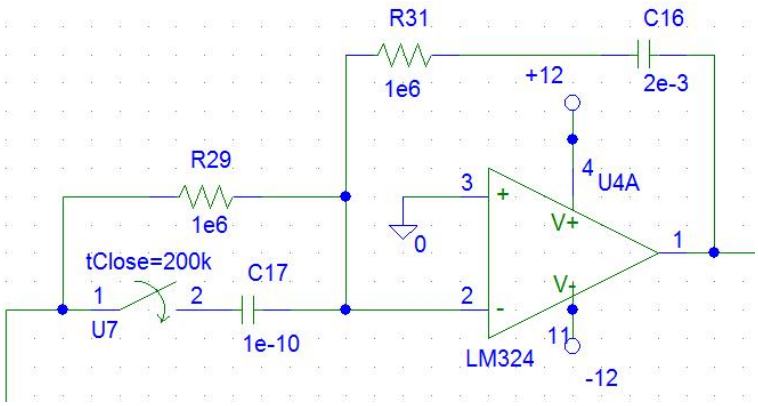


Figure 3.19: PI Controller Schematic

$$G_C(s) = \frac{K_d s^2 + K_p s + K_i}{s} \tag{3.14}$$

The controllers were simulated with thermal system parameters obtained from the system identification tests. Linear control schemes were compared to a bang-bang controller. The rise time, steady state errors, steady state ramp rates in power drawn for each test were also found.

For each simulation, two linear controllers were plotted on the same graph, and the bang-bang controller was plotted separately. The $V_{heater}$ was plotted for each controller where $V_{heater}$ corresponds to the voltage on the load (heater) resistor. $V_{heater}$ is plotted with thicker lines than the $V_{room}$, and $V_{room}$ has the same color for the corresponding controller. $V_{ambient}$ is also plotted in black for each controller. The estimated 25 °C and 32 °C systems were tested using the set-points from the original experiment. A sinusoidal ambient temperature was also used with ±2.5 °C range and period=20000 seconds. Since the temperature range was close to the identification point, it was assumed that the thermal model was still valid. The controllers all converged to the correct $V_{room}$ set-point. However, it is clear that linear controllers peak voltage demand at steady state is significantly lower than bang-bang controller.

### 3.2.7 Simulations with Constant Ambient Temperature

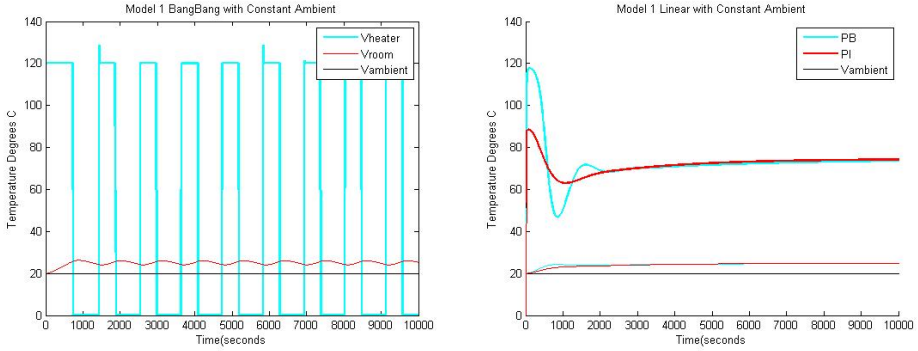


(a) Bang-Bang (b) Linear

Figure 3.20: 25 °C Simulations with Constant Ambient

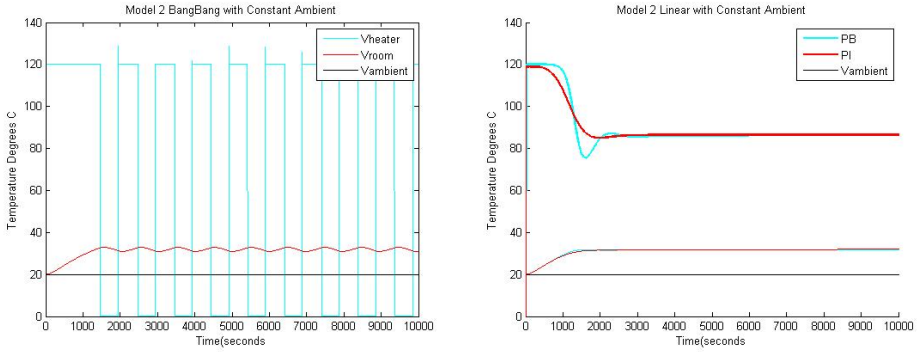


(a) Bang-Bang (b) Linear

Figure 3.21: 32 °C Simulations with Constant Ambient

The peak power demand reduction can be seen by comparing the maximum steady state voltage between linear and bang-bang controllers. In all tests the steady state operating voltage is the same for both linear controllers. Plots with 25 °C and 32 °C set-points can be seen in Fig. 3.20 and Fig. 3.21. For the 32 °C system, the bang-bang controller uses a $V_{heater}$ of $120V$ at steady state while the linear controllers converge to $80V$. The peak voltage reduction is approximately 33% for this test. With a lower operating point, the voltage reduction is greater, and the reduction is much lower for 25 °C for this reason. Since this voltage was applied to a resistor, the current will also be smaller at the same rate as voltage. Using $P = \frac{V_2}{R}$ formula, this translates into 55.6% peak power demand reduction for 32 °C.

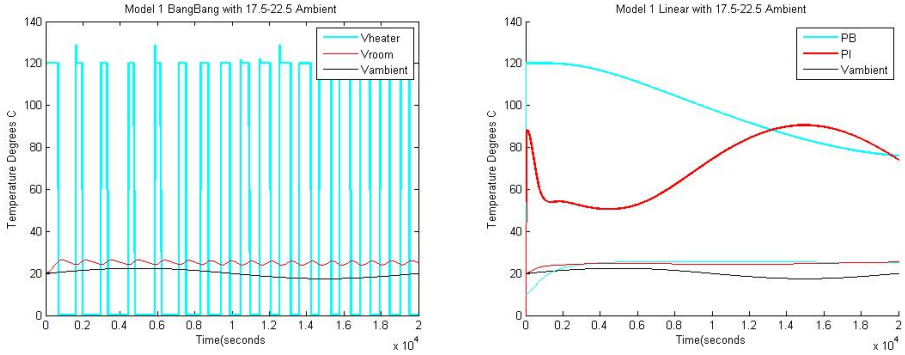


(a) Bang-Bang (b) Linear

Figure 3.22: 25 °C Simulations with 17.5 – 22.5 °C Ambient

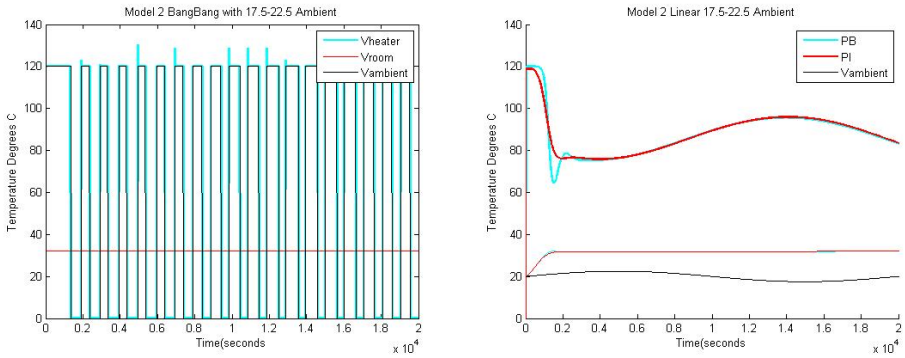


(a) Bang-Bang (b) Linear

Figure 3.23: 32 °C Simulations with 17.5 – 22.5 °C Ambient

### 3.2.8 Simulations with 17.5 ° – 22.5 °C Variable Ambient Temperature

The next test had a variable ambient temperature. The linear controller adjusts the operating voltage to match the ambient temperature based on the changes in the feedback control signal. The bang-bang controller changes the duty cycle in order to accomplish this, but always demands the maximum voltage which is 120 Volts. Plots of simulations can be seen in Fig. 3.22 and Fig. 3.23.

### 3.2.9 Controller Performance Comparisons

Resulting performance was evaluated for both 25 °C and 32 °C systems as seen in Tables 3.3 and 3.4. Rise time was calculated as the time it takes $V_{room}$ to reach

Table 3.3: 25 °C Rise Time, Max and Min Errors

| Controller | Set Point °C | Ambient °C | Rise Time (Seconds) | Max Error °C | Min Error °C |
|---|---|---|---|---|---|
| Phase Boost | 25 | 20 | 596 | 0.04 | 0.04 |
| PI | 25 | 20 | 2312 | 0.05 | 0.05 |
| BangBang | 25 | 20 | 507 | 1.04 | 0.91 |
| Phase Boost | 25 | $17.5 - 22.5$ | 556 | 0.36 | 0.44 |
| PI | 25 | $17.5 - 22.5$ | 1368 | 0.52 | 0.62 |
| BangBang | 25 | $17.5 - 22.5$ | 485 | 1.40 | 1.11 |

Table 3.4: 32 °C Rise Time, Max and Min Errors

| Controller | Set Point °C | Ambient °C | Rise Time (Seconds) | Max Error °C | Min Error °C |
|---|---|---|---|---|---|
| Phase Boost | 32 | 20 | 1159 | 0.04 | 0.04 |
| PI | 32 | 20 | 1280 | 0.05 | 0.05 |
| BangBang | 32 | 20 | 1147 | 0.93 | 1.04 |
| Phase Boost | 32 | $17.5 - 22.5$ | 1074 | 0.23 | 0.32 |
| PI | 32 | $17.5 - 22.5$ | 1169 | 0.32 | 0.41 |
| BangBang | 32 | $17.5 - 22.5$ | 1062 | 1.06 | 1.18 |

95% of the set point temperature. The maximum and minimum errors for steady state operations were also calculated. All controllers performed well and had negligible errors at steady state. The PI controller converged much slower for the 25 °C, but stayed within a close tolerance once it converged. The phase boost controller had the least error margins and slightly longer rise times than the bang-bang controller. The bang-bang controller always had the largest error because of the turn on and turns off temperatures from the Schmitt trigger. Decreasing the temperature range of a

Table 3.5: 25 °C Max and Min Slope

| Controller | Set Point °C | Ambient °C | Volt/Hour Max Slope | Volt/Hour Min Slope |
|---|---|---|---|---|
| Phase Boost | 25 | $17.5 - 22.5$ | 0.44 | $-0.49$ |
| PI | 25 | $17.5 - 22.5$ | 0.65 | $-0.74$ |
| BangBang | 25 | $17.5 - 22.5$ | 2721.50 | 2721.50 |

bang-bang controller apparently requires more switching which results in more stress on the heating element.

### 3.2.10 Maximum and Minimum Demand Ramp Rates

The power demand ramp rates or voltage slopes were also measured for the controllers in Volts/Hour for 25 °C as seen in Table 3.5. The results were also pretty similar with 32 °C. These voltage slopes were calculated for the steady state operation. The ramp rates were smallest with the phase boost controller. On the other hand, the ramp rate was always large for bang-bang controllers, even when the outside temperature is constant. The slopes were close to zero for linear controllers at steady state with a constant ambient temperature testing.

# CHAPTER 4: EXPERIMENTAL RESULTS AND DISCUSSION

In order to experimentally validate the control methodology of this thesis a linear controller was built and tested with a proportional-integral controller. The estimated thermal system from a 25 °C identification was used. A buck converter was implemented with the circuit seen in Fig. 4.1. The DC power supply was limited to $86VDC$, the buck converter parameters were different than the parameters used in the PSpice system. The DC voltage supply was achieved with a 2:1 step-down transformer and full wave rectifier. Therefore a new phase margin calculation was needed that took into account the following power stage, and new controller parameters to create a valid controller.

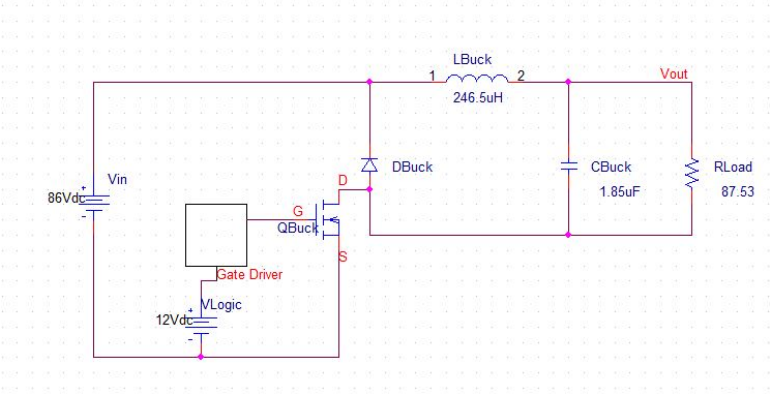


Figure 4.1: Linear Controller - Buck Converter Power Stage

An Arduino Uno R3 was used to adjust the $V_{GS}$ duty cycle of the buck converter. A picture of the instrumentation and circuit used can be seen in Fig.4.2 and Fig.4.3 respectively. An opto-isolator was used to drive a MOSFET firing circuit for the buck converter as seen in Fig. A.3 of the Appendix.

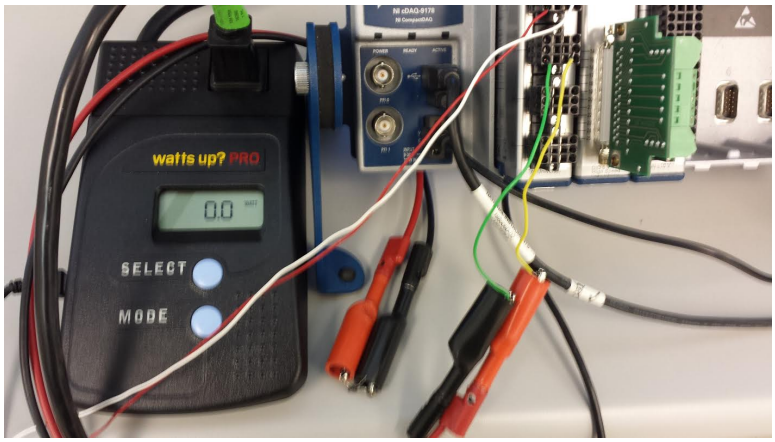


Figure 4.2: Linear Controller Instrumentation

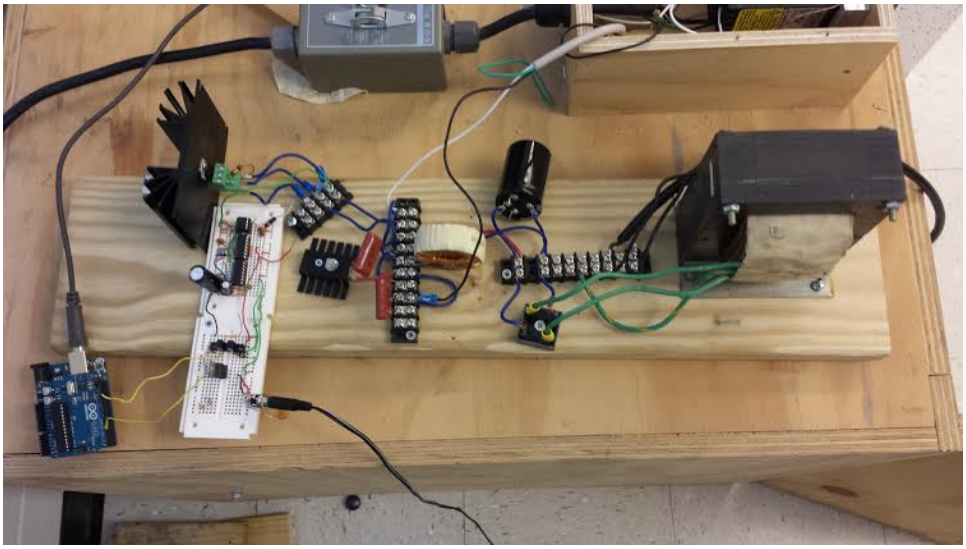

Figure 4.3: Linear Controller Circuit

The output voltage $V_{out}$ can be found with $V_{out} = DV_{in}$ where $D$ is the $V_{GS}$ duty cycle. $V_{GS}$ changes linearly with a digital adjustment of a PWM on the Arduino. A plot of measured $V_{GS}$ duty cycles can be seen in Fig. 4.4.

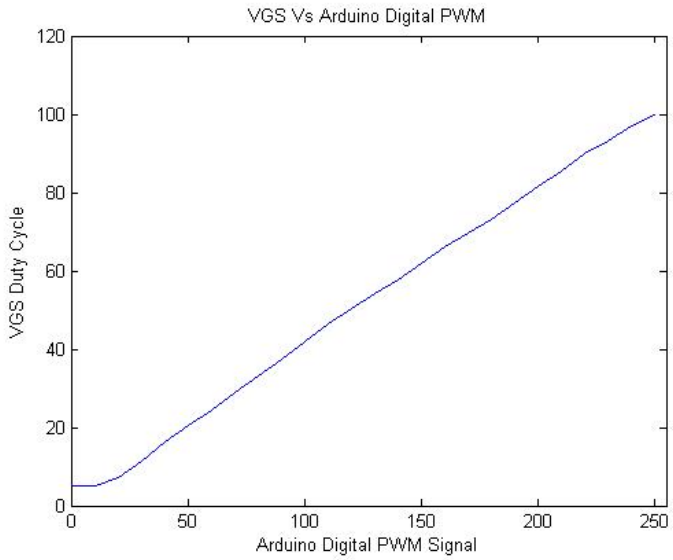


Figure 4.4: VGS Duty Cycle Control with Arduino Uno R3

The Arduino PWM pin was adjusted from 0 to 250 to achieve the desired $V_{GS}$ range. Sample MOSFET $V_{GS}$ and $V_{DS}$ screen captures can be seen in Fig. 4.5 and Fig. 4.6. A switching frequency of $120kHz$ was used for the MOSFET to ensure continuous conduction mode (CCM). The AC power draw for the system including losses was measured with a Watts Up? Pro meter. A sampling time of 2 seconds was used for the test. The reason for this is as follows. The crossover frequency for the overall system was selected as $0.002Hz$. In practice, cutoff frequency needs to be at least $10-20$ times larger than this value. If we select $0.05Hz$ for the cutoff frequency, then the minimum sampling frequency based on Shannon's sampling theorem needs to be $0.1Hz$ or a sampling period of 10 seconds. A selection of 2 seconds of sampling interval comfortably satisfies this requirement [27].

Power readings were used to find the operating voltage of each controller. A power offset was observed due to losses in the transformer, MOSFET, and diode.

The theoretical power stage power was calculated using $V_{in}D = V_{out}$ to calculate the approximate voltage applied to the heating element and compared to the experiment data in Fig. 4.7.

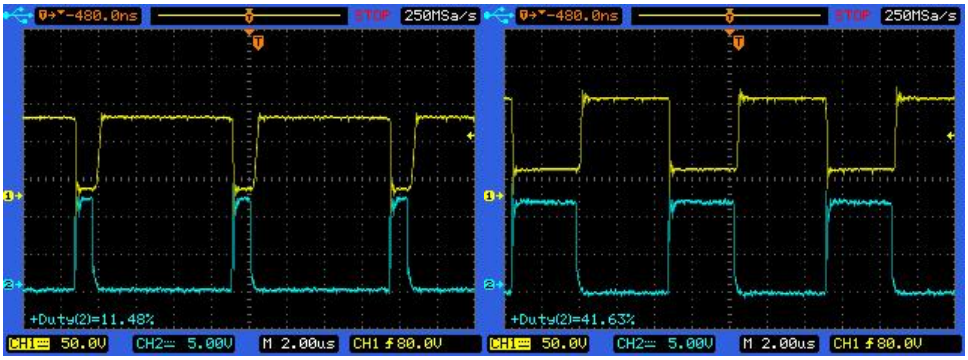


(a) 30 Logic Signal (b) 100 Logic Signal

Figure 4.5: Arduino PWM Signal $V_{GS}$ (Blue) and $V_{DS}$ (Yellow)

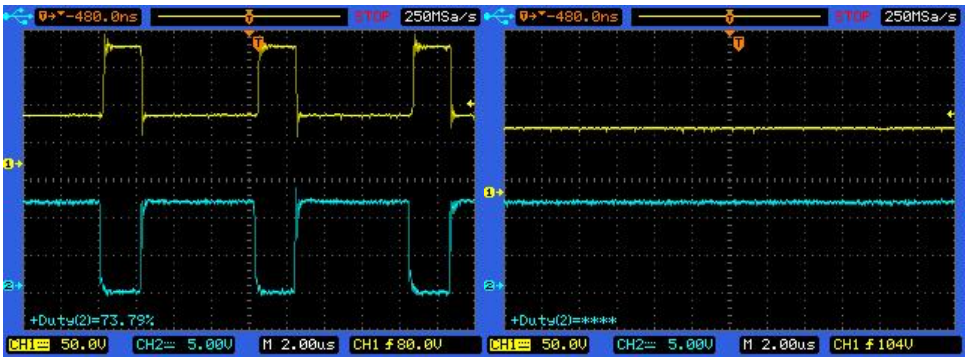


(a) 180 Logic Signal (b) 250 Logic Signal

Figure 4.6: Arduino PWM Signal $V_{GS}$ (Blue) and $V_{DS}$ (Yellow)

Because the power stage has a very fast time in comparison to the system, its transfer function is assumed to be $\frac{V_{out}}{V_{in}} = D$. The thermal system parameters from a previous estimation explained in the methodology chapter were used. The thermal estimation used Honeywell $td5a^{TM}$ rtd sensors and includes the time constant of these sensors. A 60 ° phase margin was targeted because it provides smooth, nicely damped settling characteristic. The steady state error is theoretically zero due to the integrator in the PI controller. Set-points of 25 °C and 27 °C were used with a simple

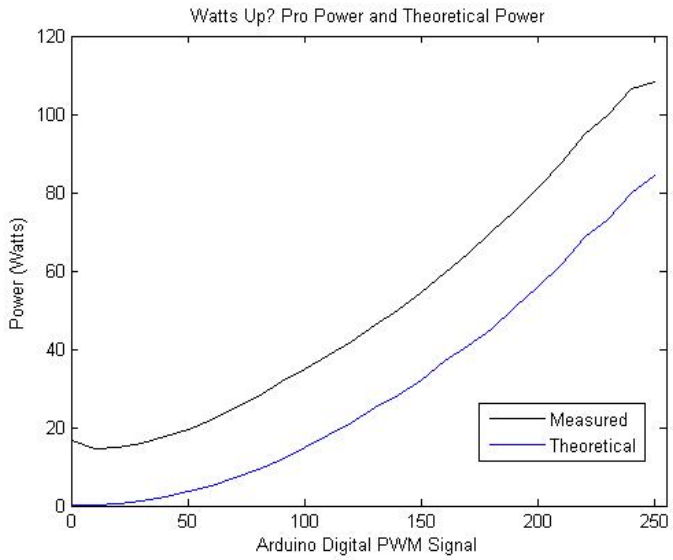


Figure 4.7: Watts Up? Pro Power and Theoretical Buck Converter Power

PI controller to create the desired phase margin. The controller was implemented in $LabVIEW^{TM}$ with three primary actions. The power was read with a Watts Up? Pro meter, enclosure temperature and ambient temperature were measured with td5a rtds, and a digital PWM signal from Arduino was sent to a MOSFET driver to control the buck converter. A $LabVIEW^{TM}$ block diagram of the controller can be seen in Fig. A.2 of the Appendix. The chosen PI designs for each temperature set-point can be seen in Table 4.1, with a Matlab file for calculations in Appendix A. Bode plots for each controller can be seen in Fig. 4.8. In the phase margin calculation the nonlinear power was linearized by multiplying the open loop transfer function with $\frac{2V_{out}}{R}$. The linearization is achieved with the derivative of the power seen in (4.1) and (4.2).

$$P = \frac{V_{out}^2}{R} \tag{4.1}$$

$$\frac{dP}{dV_{out}} = \frac{2V_{out}}{R} \tag{4.2}$$

Table 4.1: Phase Margin for Each Trial

| Set-point | Pk | Pi | Steady Power (Watts) | Operating (Volts) | Margin (Degrees) |
|---|---|---|---|---|---|
| 25 | 2 | $1e-3$ | 35.8 | 36.2 | 64 |
| 25 | 2 | $1.5e-3$ | 35.1 | 36.2 | 59.2 |
| 25 | 2 | $2e-3$ | 39.3 | 39.9 | 53.1 |
| 27 | 2 | $7.5e-4$ | 50 | 49.6 | 59 |
| 27 | 2 | $5e-4$ | 53.1 | 53.15 | 59.2 |
| 27 | 2 | $1e-3$ | 54.6 | 53.15 | 55.6 |

The theoretical temperature response was also calculated and plotted for each phase margin. The power stage transfer function was simplified due to its fast response as mentioned earlier and a 25 ° thermal system transfer function was used as seen in Fig. 4.9. In the simulink block diagram the PI system (Controller) output signal is applied to a low pass filter (Filter) block, and a PWM reduction block. These items were also present in the real system. After the PWM block, the control signal is applied to a DC power supply (Buck Conv) and converted to a power signal applied to the thermal transfer function (Transfer Fcn3).

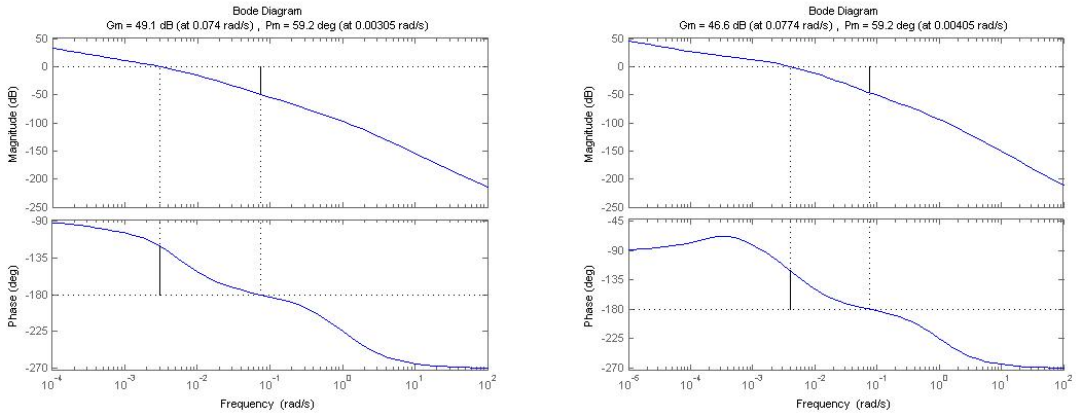


(a) 25 °C (b) 27 °C

Figure 4.8: Open Loop Bode Plots with 59 ° Phase Margin for Both Set-Points

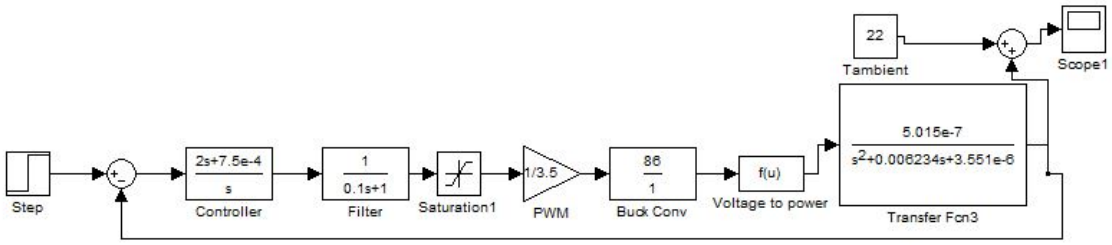


Figure 4.9: Temperature Response Calculation in Matlab / Simulink

Once the test was performed plots of Power/$V_{Control}$ and temperature for each test were generated. $V_{Control}$ is a signal between $0-250$ that correlates to the operating voltage of the buck converter. The 25 °C set-point temperature dynamics can be seen in Fig. 4.10, 4.11, and 4.12. Associated power and $V_{Control}$ dynamics are also shown. The phase margin of close to 50 degrees in test 2 shows the largest overshoot and worst performance for this set-point. The test closest to 60 ° phase margin had the smoothest settling response. Therefore, an ideal $P_i$ term would be between $10e-4$ and $15e-4$ for 25 °C set-point.

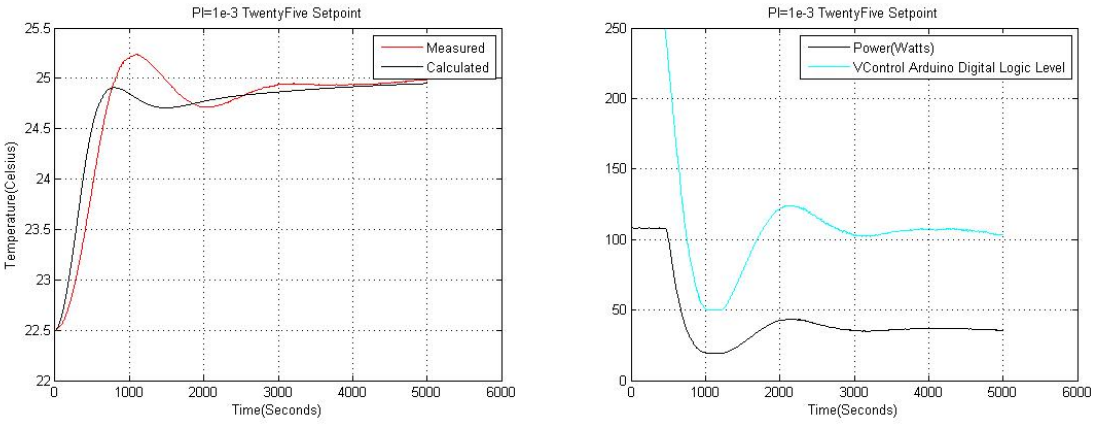


(a) Temperature

(b) Power(Black) and $V_{Control}$(Teal)

Figure 4.10: Measured and Calculated Data for 25 °C Set-point and $P_i = 10e-4$)

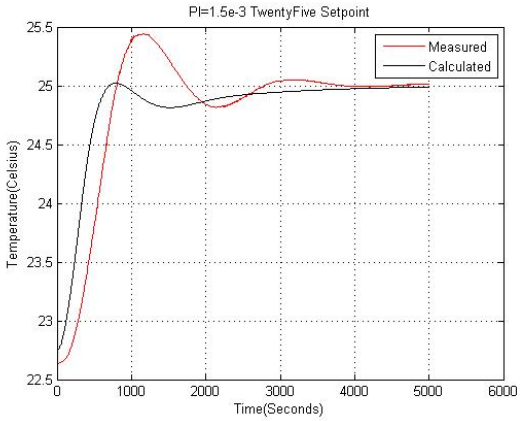


(a) Temperature

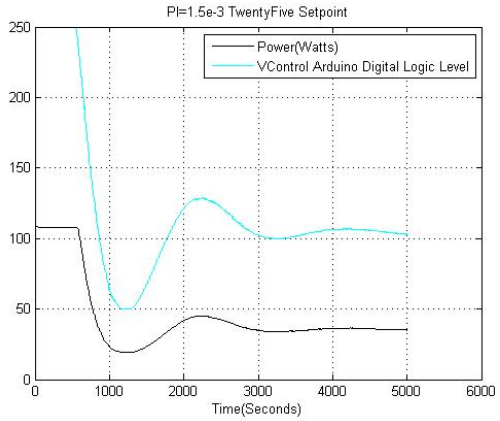


(b) Power(Black) and $V_{Control}$(Teal)

Figure 4.11: Measured and Calculated Data for 25 °C Set-point and $P_i = 15e - 4$)

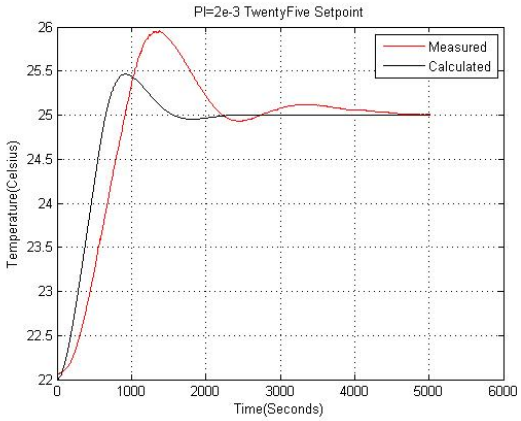


(a) Temperature

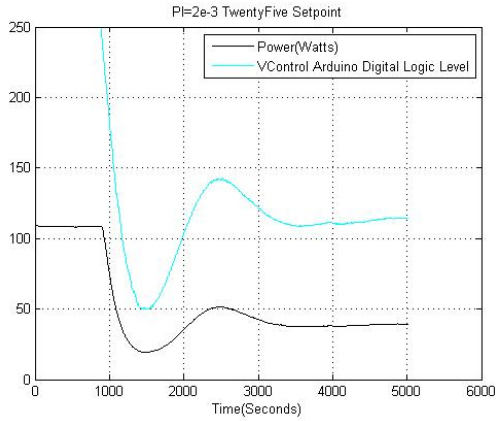


(b) Power(Black) and $V_{Control}$(Teal)

Figure 4.12: Measured and Calculated Data for 25 °C Set-point and $P_i = 20e - 4$)

A test using a 27 °C set-point was also performed using the 25 °C thermal identification model. The 27 °C set-point system temperature dynamics for different values of $P_i$ terms can be seen in Fig. 4.13, 4.14, and 4.15. 27 °C power and $V_{Control}$ dynamics are also shown. The smoothest settling was observed with $P_i = 7.5e-4$. The 25 °C thermal system was initially used to generate the appropriate $P_i$ and $P_k$ terms. When choosing a $P_i$ term it was found that increasing $P_i$ resulted in larger overshoots which is primarily due to decreasing phase margins below 60 °. Simulated temperature responses were also plotted on the same graphs using the 25 °C thermal system. However, the simulink model had a different "Voltage-to-power" block due to the different operating voltages listed in Table 4.1. Because the PI controller only has a single pole at the origin and a single zero, the controller may not be able to perfectly control a more complicated system. It may be useful to use additional poles or zeros in a future work with a lead compensator (phase boost) controller, as used in the PSpice simulations. As it can be seen from the theoretical and experimental temperature plots the experimental system is more under-damped in comparison to calculated system dynamics [28].

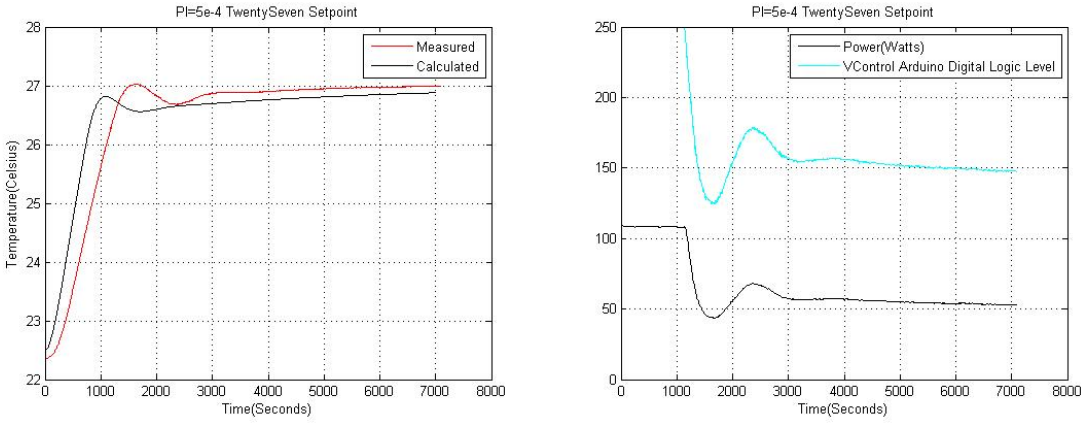


(a) Temperature

(b) Power(Black) and $V_{Control}$(Teal)

Figure 4.13: Measured and Calculated Data for 27 °C Set-point and $P_i = 5e-4$)

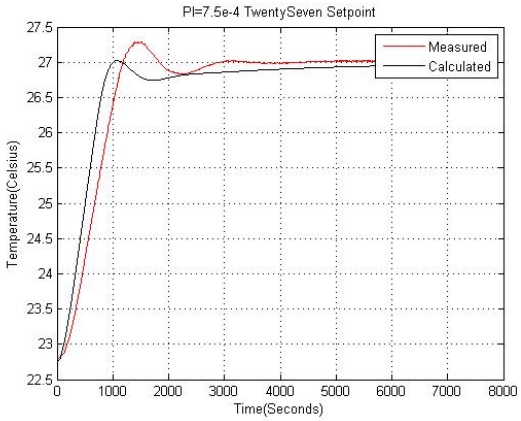


(a) Temperature

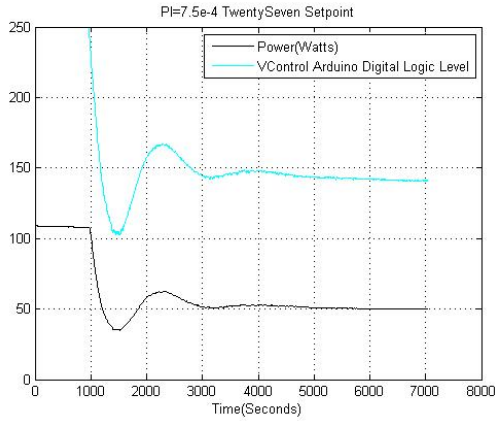


(b) Power(Black) and $V_{Control}$(Teal)

Figure 4.14: Measured and Calculated Data for 27 °C Set-point and $P_i = 7.5e - 4$)

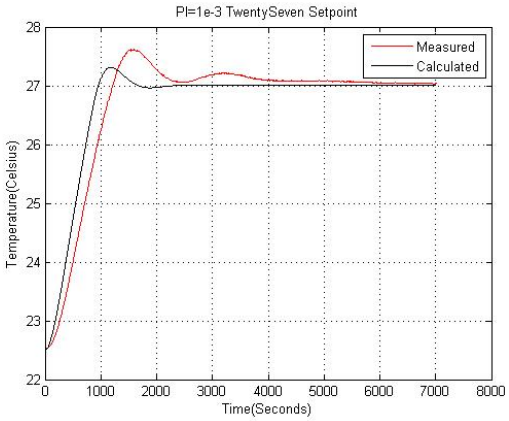


(a) Temperature

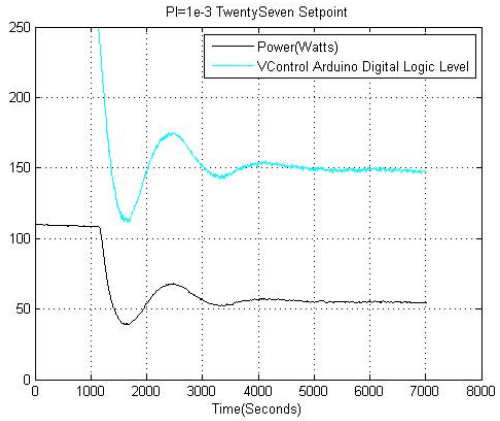


(b) Power(Black) and $V_{Control}$(Teal)

Figure 4.15: Measured and Calculated Data for 27 °C Set-point and $P_i = 10e - 4$)

# CHAPTER 5: CONCLUSION AND FUTURE WORK

This thesis implemented a three part method for linearizing an electric space heating load. A successful thermal estimation was performed using steady-state operating data for an enclosure with fits greater than 80%. A controller was designed with a buck converter power stage that leveled the load that resulted in a constant DC voltage being applied to a load at steady state. The controller was adjusted to achieve a 60 ° phase margin and tested to verify smooth control, the final experiment had similar overshoot and settling times for each test.

A temperature set-point of 27 °C was used to show that the 25 °C thermal model was still valid for different set-points. For the 27 °C set-point the steady state operating voltage was needed, and successfully used in the experiment. Overall the method provided five major benefits over utilizing standard bang-bang controllers:

1. Reduced peak power demand
2. Smoothed demand ramp rates
3. Eliminated inrush currents
4. Achieved constant power regardless of voltage fluctuations
5. Improved temperature comfort levels

Future research for this project includes changing the ambient temperature during the experiment in order to model outdoor conditions. In addition, more complicated controllers as well as other power converters such as an AC chopper can also be utilized for more efficient system performance.

# BIBLIOGRAPHY

[1] Matthew Cordaro, "Understanding base load power,"White paper, October, 2008.

[2] Ned Mohan, Electric Power Systems: A First Course, John Wiley & Sons, 2012.

[3] Joseph Eto, "The past, present, and future of us utility demand side management programs," Revue de lnergie, , no. 483, 1996.

[4] M. Alizadeh, Xiao Li, Zhifang Wang, A. Scaglione, and R. Melton, "Demand-side management in the smart grid: Information processing for the power switch," Signal Processing Magazine, IEEE, vol. 29, no. 5, pp. 5567, 2012, ID: 1.

[5] Guy R. Newsham and Brent G. Bowker, "The eect of utility time-varying pricing and load control strategies on residential summer peak electricity use: A review," Energy Policy, vol. 38, no. 7, pp. 32893296, 7 2010.

[6] S. El-Ferik, S. A. Hussain, and F. M. Al-Sunni, "Identication of physically based models of residential air-conditioners for direct load control management," in Control Conference, 2004. 5th Asian, 2004, vol. 3, pp. 20792087 Vol.3, ID: 1.

[7] J. Kondoh, Ning Lu, and D. J. Hammerstrom, "An evaluation of the water heater load potential for providing regulation service," Power Systems, IEEE Transactions on, vol. 26, no. 3, pp. 13091316, 2011, ID: 1.

[8] D. S. Callaway, "Can smaller loads be protably engaged in power system services?," in Power and Energy Society General Meeting, 2011 IEEE, 2011, pp. 13, ID: 1.

[9] Guy R. Newsham, Benjamin J. Birt, and Ian H. Rowlands, "A comparison of four methods to evaluate the eect of a utility residential air-conditioner load control program on peak electricity use," Energy Policy, vol. 39, no. 10, pp. 63766389, 10 2011.

[10] Ning Lu, Pengwei Du, and Y. V. Makarov, "The potential of thermostatically controlled appliances for intra-hour energy storage applications," in Power and Energy Society General Meeting, 2012 IEEE, 2012, pp. 16, ID: 1.

[11] M. H. Nehrir, Runmin Jia, D. A. Pierre, and D. J. Hammerstrom, "Power management of aggregate electric water heater loads by voltage control," in Power Engineering Society General Meeting, 2007. IEEE, 2007, pp. 16, ID: 1.

[12] N. Baghina, I. Lampropoulos, B. Asare-Bediako, W. L. Kling, and P. F. Ribeiro, "Predictive control of a domestic freezer for real-time demand response applications," in Innovative Smart Grid Technologies (ISGT Europe), 2012 3rd IEEE PES International Conference and Exhibition on, 2012, pp. 18, ID: 1.

[13] Nikolai A. Sinitsyn, Soumya Kundu, and Scott Backhaus, "Safe protocols for generating power pulses with heterogeneous populations of thermostatically controlled loads," Energy Conversion and Management, vol. 67, no. 0, pp. 297308, 3 2013.

[14] U.S. Energy Information Administration (USEIA). (05/28/2013), "Heating and cooling no longer majority of u.s. home energy use," Available: http://www.eia.gov/todayinenergy/detail.cfm?id=10271. DOI: 06/25/2014.

[15] Rich Brown, "Us building-sector energy eciency potential," Lawrence Berkeley National Laboratory, 2008.

[16] Torsten Broeer, Jason Fuller, Francis Tuner, David Chassin, and Ned Djilali, "Modeling framework and validation of a smart grid and demand response system for wind power integration," Applied Energy, vol. 113, no. 0, pp. 199207, 1 2014.

[17] WireTronic Inc. (12/07/2013), "Nicrome 80 & other resistance alloys - technical data & properties," Available: http://www.wiretron.com/nicrdat.html;. DOI: 07/03/2014.

[18] H. Dean Venable, "The k factor: A new mathematical tool for stability analysis and synthesis," Citeseer.

[19] P. Radecki and B. Hencey, "Online building thermal parameter estimation via unscented kalman ltering," in American Control Conference (ACC), 2012, 2012, pp. 30563062, ID: 1.

[20] Ion Hazyuk, Christian Ghiaus, and David Penhouet, "Optimal temperature control of intermittently heated buildings using model predictive control: Part i building modeling," Building and Environment, vol. 51, no. 0, pp. 379-387, 5 2012.

[21] Aaron Smith, Rogelio Luck, and Pedro J. Mago, "Integrated parameter estimation of multi-component thermal systems with demonstration on a combined heat and power system," ISA transactions, vol. 51, no. 4, pp. 507513, 7 2012.

[22] Y. Cengel, Introduction to THermodynamics and Heat Transfer, McGraw-Hill Science/Engineering/Math, 2007.

[23] A. Wills and B. Ninness, "On gradient-based search for multivariable system estimates," Automatic Control, IEEE Transactions on, vol. 53, no. 1, pp. 298306, 2008, ID: 1.

[24] K. Levenberg, "A method for the solution of certain problems in least squares," IEEE Transactions on Circuits and Systems, vol. CAS-26, 1979.

[25] "Matlab 2012a system identication toolbox," .

[26] Ned Mohan, Power Electronics A First Course, John Wiley & Sons, Inc., MA, 1 edition, 2012.

[27] Lee Holland, H. Bora Karayaka, Martin L. Tanaka, and Aaron Ball, "An empirical method for estimating thermal system parameters based on operating data in smart grids," in Innovative Smart Grid Technologies Conference (ISGT), 2014 IEEE PES, 2014, pp. 15, ID: 1.

[28] Lee Holland, H. Bora Karayaka, Martin L. Tanaka, and Aaron Ball, "An investigation of parametric load leveling control methodologies for resistive heaters in smart grids," in Green Technologies Conference (GreenTech), 2014 Sixth Annual IEEE, 2014, pp. 8792, ID: 1.

# Appendices

# APPENDIX A: SOURCE CODE

```
%First order thermal circuit state space model for
    Identification
function [A,B,C,D] = therm1(par,ts)
R2 = par(1);
C1 = par(2);
%System Dynamics:
A = -1/(R2*C1);
B = [1/C1 1/(R2*C1)];
C = 1;
D = [0 0];
K = 0;

if ts>0 % Sample the model with sample time Ts
    s = expm([[A B]*ts; zeros(2,3)]);
    A = s(1,1);
    B = s(1,2:3);
end
```

```
%Second order thermal circuit state space model for
    Identification
function [A,B,C,D,K] = therm2(par,ts)
R2 = par(1);
C1 = par(2);
R3 = par(3);
C2 = par(4);
%System dynamics:
A = [-1/(R2*C1) 1/(R2*C1);1/(R2*C2) -(1/(R2*C2)+1/(R3*C2))
    ];
B = [1/C1 0;0 1/(R3*C2)];
C = [0 1];
D = [0 0];
K = [0;0];

if ts>0 % Sample the model with sample time Ts
    s = expm([[A B]*ts; zeros(2,4)]);
    A = s(1:2,1:2);
    B = s(1:2,3:4);
end
```

```
%Thermal system identification with estimation/validation
    calculations
clear all
close all
load J10ONData.mat
TintgnaJ10=[10000 16000 16000 32100]%Initial conditions
    for parameters
GuessgnaJ10=[15, 150, .15, 150]%Window for estimation and
    validation

Ts=2;%Sampling time for time domain conversion
%iddata creates time domain system with:
    %J10Tout (Output)- Temperature inside Enclosure
    %J10PinR (Input) - Power into system (applied to
        resistance heater)
    %J10TinR (Input) - Ambient Temperature
lee=iddata(J10Tout(:,3),[J10PinR(1:34273,1) J10TinR],Ts);
ze=lee(TintgnaJ10(1,1):TintgnaJ10(1,2));%Estimation Window
par_guess=GuessgnaJ10(1,:);%Initial Conditions

%idgrey setup
dcmm = idgrey('therm2',par_guess,'cd',{},0)
opt = greyestOptions('Display','on','InitialState','auto'
    ,...
                     'DisturbanceModel','none','
                       SearchMethod','gna');
dcmm = greyest(ze,dcmm,opt)%Estimation

%Final Parameters:
R2=dcmm.B(1,1)/dcmm.A(1,2)
C1=1/dcmm.B(1,1)
C2=1/(R2*dcmm.A(2,1))
R3=1/(C2*dcmm.B(2,2))
par_final= [R2 C1 R3 C2];

[y0,fit0,x0] = compare(ze,dcmm)%Estimation fit

dcmm1 = idgrey('therm2',par_final,'cd',{},0);
compare(ze,dcmm1)%Estimation fit plot
zv=lee(TintgnaJ10(1,3):TintgnaJ10(1,4));%Validation Window

[y1,fit1,x0] = compare(zv,dcmm1)%Validation fit
figure
compare(zv,dcmm1)%Validation fit plot
```

```
%PI Phase Margin Pk and PI parameter script for 60 degree
    phase margin
%This is a script that was used to find the Conroller /
    Open loop transfer
%function of the phase boost controller

%Initial Conditions
fcutoff=9*10^-4; %Cutoff Frequency for the system
GL_Phase_Offset=0;
GPWM_Mag=1/3.7;%Arduino range over PWM Voltage
R1=10^6;%Ohms -- Not Needed for PI
wcutoff=fcutoff*2*pi;%rad/s
%Estimation for 25 degree set-point
A=[-0.0012655 0.0012655; 4.8711e-05 -0.0041];
B=[0.0082869 0;0 0.0040513];
C=[0 1];
D=[0 0];
%Parameters for Physical Power Stage / Buck Converter
Vin=86; %Input voltage
Vo=36.2; %Buck operating voltage
L=246*10^-6;%Henry's
r=0.1;%Ohms
Cb=1.875*10^-6;%Ferads
R=87.53;%Ohms - Rheater
%PI Parameters - Change to adjust Phase Margin
Pk=2;
Pi=15e-4;

%Transfer Functions for Each System
[NUM1tf, DEN1tf]=ss2tf(A,B,C,D,1);%Thermal System
therm=tf(NUM1tf,DEN1tf);

Num_Buck_tf=Vin*[r*Cb 1];%Power Stage / Buck Converter
Den_Buck_tf=L*Cb*[1 (1/(R*Cb)+r/L) 1/(L*Cb)];
BuckTransfer=tf(Num_Buck_tf,Den_Buck_tf);

GCNum=Pk*[1 Pi/Pk];%PI transfer function
GCDem=[1 0];
GCtf=tf(GCNum,GCDem);

RC=1;%Mosfet Driver RC Filter
GFnum=[1];
GFden=[RC 1];
GF=tf(GFnum,GFden);
```

```
43
44 %Individual system magnitute and phase
45 [GTherm_Mag, GTherm_Phas_fc]=bode(therm,wcutoff)%Thermal
46 Gthermmagdb=20*log10(GTherm_Mag)%therm mag1 at fc in db
47
48 [GBuck_Mag, GBuck_Phase_fc]=bode(BuckTransfer,wcutoff)%
   Power stage
49 GBuckmagdb=20*log10(GBuck_Mag)%buck mag1 at fc in db
50
51 GC_Mag=1/(GPWM_Mag*(2*Vo/R)*GBuck_Mag*GTherm_Mag)%Open
   loop gain
52
53 %The total open loop gain and phase:
54 GL_Mag=GC_Mag * GPWM_Mag * GBuck_Mag * GTherm_Mag * 2*Vo/R
   ;
55 GL_Phase_fc=-120+GL_Phase_Offset;%degrees
56
57 %Phase Boost Used
58 Phi_Boost=GL_Phase_fc-GTherm_Phas_fc-GBuck_Phase_fc+90;
59
60 %Complete transfer function and Bode Plot
61 GOpenLoop=GCtf*GPWM_Mag*GF*BuckTransfer*therm*2*Vo/R;
62 figure
63 bode(GOpenLoop)
64 title('Open Loop Bode Plot')
65 margin(GOpenLoop)
66
67 %Complete system with feedback
68 GCloseLoop1=feedback(GOpenLoop,1);
69 opt=stepDataOptions;
70 opt.InputOffset=22.5;
71 opt.StepAmplitude=25;
```

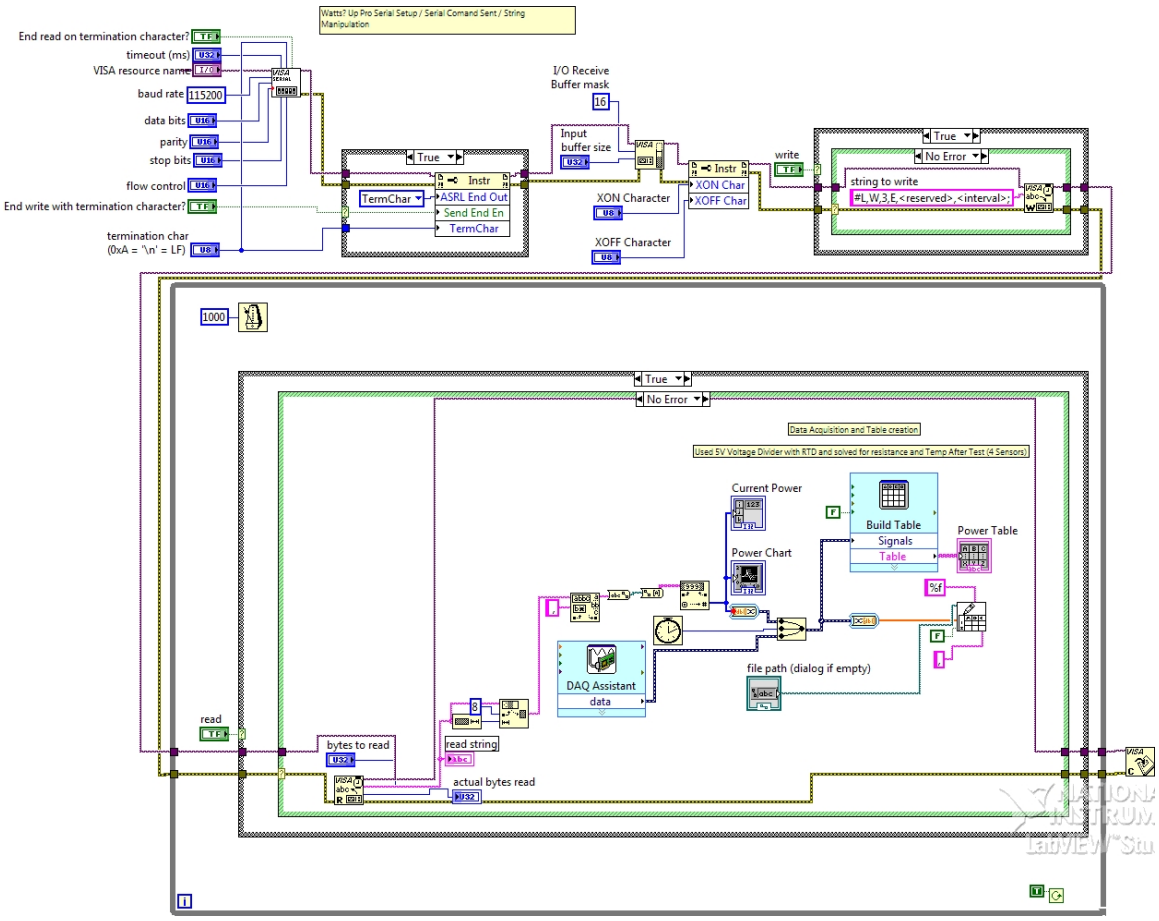


Figure A.1: Labview Block Diagram for Datalogging System Identification

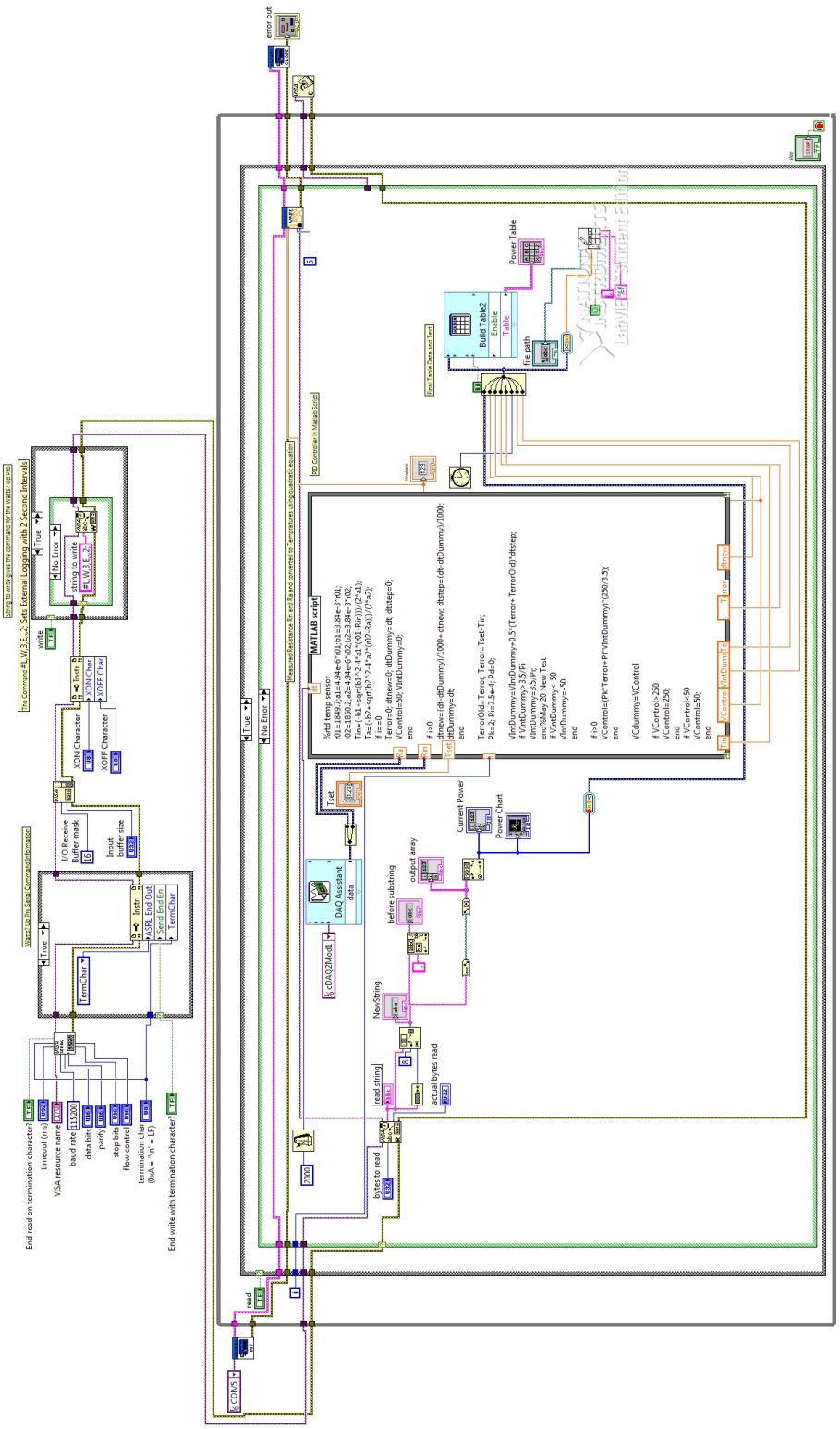

Figure A.2: Labview Block Diagram for Linear Controller with Datalogging

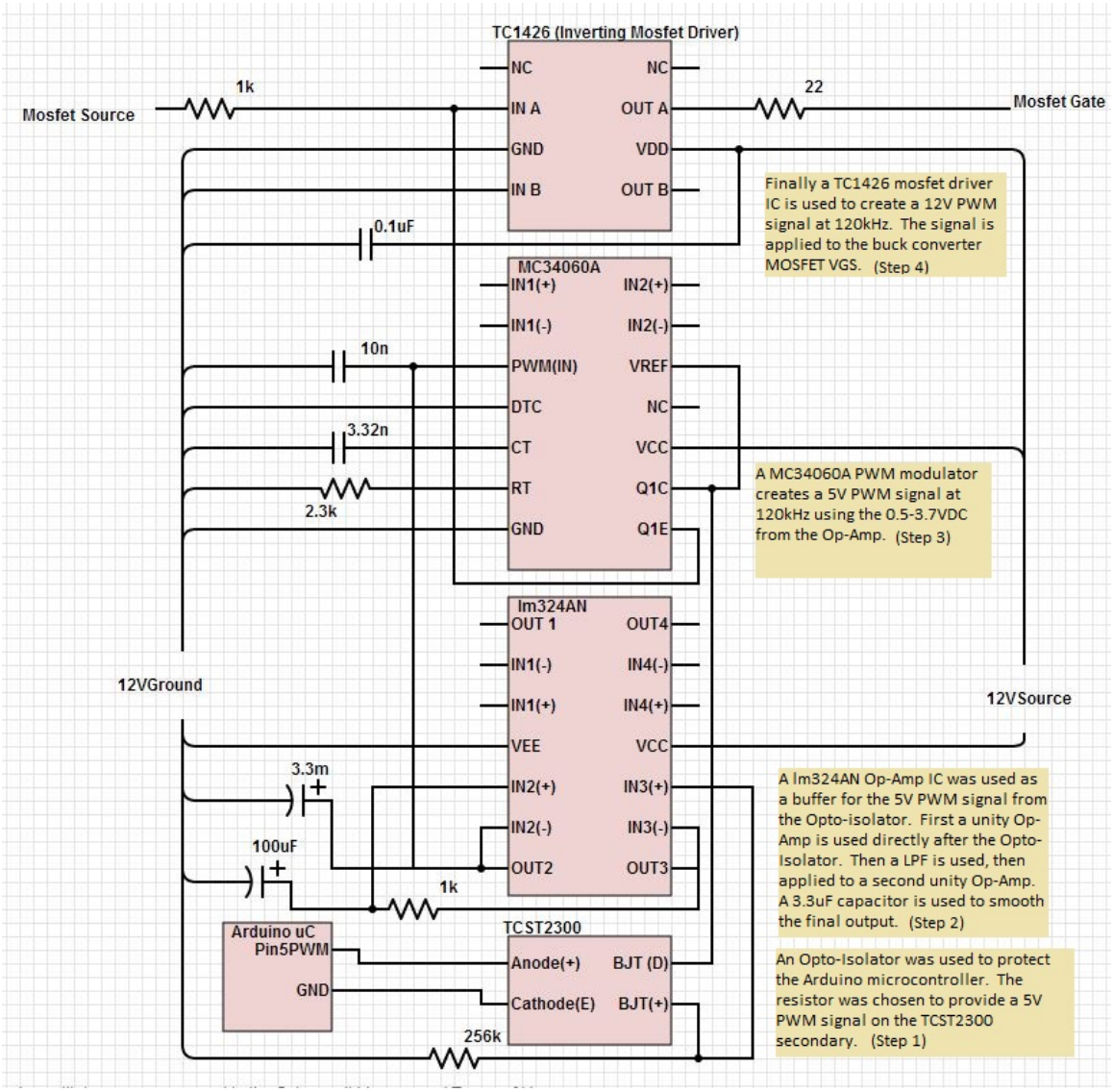


Figure A.3: Mosfet Driver Circuit for Buck Converter